THE USE OF DIFFUSE REFLECTANCE INFRARED SPECTROSCOPY IN THE STUDY OF ALUMINA

by

MARC KEVIN COLLINS

B. S., United States Military Academy, 1977

A MASTER'S THESIS

submitted in partial fulfillment of the

requirements for the degree

MASTER OF SCIENCE

Department of Chemical Engineering

KANSAS STATE UNIVERSITY
Manhattan, Kansas

1986

Approved by:

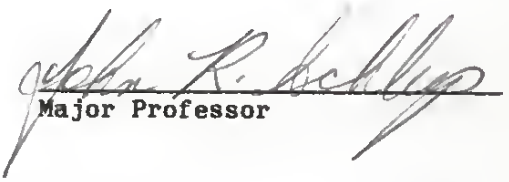

Major Professor

ACKNOWLEDGMENTS

I wish to express my sincere gratitude to all those who have helped make this thesis a reality. First, I want to aknowledge my Lord and Savior's support throughout, for everything that I accomplish is through Jesus Christ's empowering strength.

I thank Dr. John Schlup, my major professor, for the guidance, encouragement and support that he provided throughout this research. I could not have asked for a finer advisor nor could I have accomplished this research without his assistance.

I would like to thank Dr. John Matthews for the instruction that he provided on catalysis. I am also grateful for the time and effort he gave in evaluating this work as a thesis committee member.

I would like to thank Dr. William Fately for his support in both providing the equipment and expertise needed for the DRIFT spectroscopy used in this research. I am also grateful for the time and effort he gave in evaluating this work as a thesis committee member.

Dr. Robert Hammaker and Dr. Al Compaan have provided invaluble assistance in sifting through the electromagnetic phenomena with which I have dealt. Dr. Hammaker also instructed me in the use of the Perkin Elmer 180 Spectrometer.

Janet Vinduska, my typist, was superb. Her patience and support made it possible for me to complete the written portion on schedule.

Dwayne Morey machined the parts for the modified equipment.

Daimay L. Vein provided invaluble assistance in designing the modifications for the in-situ chamber. She also obtained the mid-IR DRIFT spectra.

Dr. Fang-Shyong Lai and Dr. Paul Matthewson obtained the near-IR DRIFT spectra.

IBM provided the Harrick in-situ DRIFT chamber which was the central piece of equipment to this research.

I wish to thank my loving wife, Susan, for her patience and support. None of this would have been possible without her support. I also want to thank my family for its support and encouragement.

I want to thank the United States Army which sent me to obtain a Master's Degree and which has paid for my studies.

TABLE OF CONTENTS

	Page
ACKNOWLEOGEMENTS	i
TABLE OF CONTENTS	ii
LIST OF FIGUIRES	iii
LIST OF TABLES	v
CHAPTER 1. INTROOUCTION	1
1.1 Historical Sketch	1
1.2 Objectives	2
1.3 Definitions	4
CHAPTER 2. SPECTROSCOPY	13
2.1 Transmission Infrared	14
2.2 Emission Infrared	19
2.3 Photoacoustic Infrared	20
2.4 Oiffuse Reflectance Infrared Fourier Transform	20
CHAPTER 3. THE INTERACTION OF RADIATION WITH MATTER	33
3.1 Classical analysis of interaction of electromagnetic radiation and matter	33
3.2 The dielectric constant and the forbidden zone	36
3.3 Freshnel equations	38
CHAPTER 4 EQUIPMENT	44
4.1 In-situ spectroscopy	44
4.2 Harrick high temperature vacuum chamber	45
4.3 Modifications to equipment	48
CHAPTER 5 ALUMINA	55
5.1 Choice of initial catalyst system for study	55
5.2 Alumina	56
5.3 Preparation procedures	58
CHAPTER 6 ALUMINA SPECTRA.	60
6.1 Mid-IR region	60
6.2 Mid-IR transmission spectra of alumina	60
6.3 Mid-IR ORIFT spectra of alumina	67
6.4 Near-IR region	72
CHAPTER 7 CONCLUSIONS AND RECOMMENDATIONS	92
7.1 Conclusions	92
7.2 Recommendations	94
Appendix 1 FOURIER TRANSFORM SPECTROSCOPY	97
Appendix 2 VIEWFACTOR OF KBr WINOOW	100
Appendix 3 THERMOCOUPLE CALIBRATION	103
REFERENCES	105

LIST OF FIGURES

		Page
Figure 1.	Various photophysical processes.	6
Figure 2.	Scattering process	8
Figure 3.	Raman scattering diagram	10
Figure 4.	Transmittance spectral differences KBr vs. NUJOL mull	17
Figure 5.	Transmission wafer die	17
Figure 6.	Praying mantis accessory for diffuse reflectance spectrometry	21
Figure 7.	I and J fluxes for Kubelka-Munk theory	26
Figure 8.	Plot of dielectric constant in vicinity of absorption bond.	37
Figure 9.	The forbidden zone	37
Figure 10.	Harrick in-situ DRIFT chamber.	47
Figure 11.	Modified praying mantis accessory.	49
Figure 12.	Cradle for in-situ DRIFT chamber	50
Figure 13.	Modified base plate	52
Figure 14.	Picture of Modified Aluminum Plate for FT-IR spectrometer	53
Figure 15.	Picture of Modified praying mantis	54
Figure 16.	Picture of Modified praying mantis with in-situ DRIFT chamber	54
Figure 17.	Schematic of Alumina Phases.	57
Figure 18.	Background spectra . . . . . a) KBr windows b) KBr windows and NUJOL	78
Figure 19.	Bayerite Mid-IR Transmission Spectra	79
Figure 20.	Boehmite Mid-IR Transmission Spectra	80
Figure 21.	η-Alumina Mid-IR Transmission Spectra	81

Figure 22. γ-Alumina Mid-IR Transmission Spectra 82

Figure 23. α-Alumina Mid-IR Transmission Spectrum 83

Figure 24. Boehmite Mid-IR DRIFT Spectrum 84

Figure 25. γ-Alumina Mid-IR DRIFT Spectra 85

Figure 26. γ-Alumina (2.76% in KBr) Mid-IR DRIFT Spectrum 86

Figure 27. Bayerite Near-IR DRIFT Spectrum (Technicon 500) 87

Figure 28. Boehmite Near-IR DRIFT Spectrum (Technicon 500) 87

Figure 29. γ-Alumina Near-IR DRIFT Spectrum (Technicon 500) 88

Figure 30. α-Alumina Near-IR DRIFT Spectrum (Technicon 500) 88

Figure 31. Consolidated plot of Figures 26 to 29 89

Figure 32. Bayerite and Boehmite Near-IR DRIFT Spectrum (DIGILAB 15S) 90

Figure 33. Bayerite Near-IR DRIFT spectra, with and without specular blocker) (DIGILAB 15S) 91

Figure 34. Michaelson Interferometer 99

Figure 35. Viewfactor 102

Figure 36. Thermocouple Calibration Chart 104

LIST OF TABLES

		Page
Table 1.	Vibrational Spectroscopic Techniques	13
Table 2.	Specular reflectance from nonabsorbing surfaces . .	40
Table 3.	Reference absorption peaks (mid-IR)	61
Table 4.	Observed transmission absorption peaks (mid-IR) . .	66
Table 5.	Mid-IR DRIFT absorption peaks	69
Table 6.	Near-IR DRIFT absorption peaks (Technicon 500) . . .	76
Table 7.	Near-IR DRIFT absorption peaks (DIGILAB 15S)	76
Table 8.	Calibration Table	103

Chapter 1

Introduction

1.1 Historical Sketch

In 1958, Eichens and Pliskin pioneered the use of infrared spectroscopy to study chemisorbed species [1]. Since that time, infrared (IR) spectroscopy has become the most widely used spectroscopic method available for the study of surfaces of heterogeneous catalysts [2]. Many techniques used for studying surfaces can only yield a surface averaged value, eg. BET, titration, electrochemistry, etc. Specific sites can be distinguished, however, with infrared spectroscopy. IR spectroscopy has provided much of the current information available concerning molecular structure, eg. bond angles and lengths (gaseous species), molecular symmetry [3], and identification of catalytically important sites [4]. Many bonding states and the amount of each state have also been determined for chemisorbed species with IR spectroscopy [5].

Over the last thirty years, new techniques and equipment have been developed for infrared (IR) spectroscopy. The microcomputer has greatly enhanced the data handling and processing steps involved in spectroscopy. Certainly, the Fourier transform spectrometer represents the single most important stride forward in the development of IR equipment during this period. In the 1970s, the introduction of Fourier transform (FT) spectrometers ushered in a new era for the use of IR spectroscopy (see appendix 1). Since the entire IR spectrum is detected continuously, more radiation from the source is used at any instant.

Consequently, either a shorter scan time or a better signal-to-noise ratio (SNR) is achieved [6].

Techniques, such as diffuse reflectance spectroscopy, which previously lacked the signal intensity to provide an adequate SNR in the IR region of the spectrum became possible. Willey demonstrated the usefulness of diffuse reflectance spectroscopy in the infrared region. He utilized an interferometer and an integrating sphere [7]. In 1978, Fuller and Griffiths described an optical arrangement with parabolic mirrors for conducting diffuse reflectance infrared Fourier transform (DRIFT) spectroscopy using a commercial interferometer to study powdered samples [8]. Some recent examples of the use of DRIFT are in the study of HPLC effluents [9], pharmaceuticals [10], coals [11] and absorption of phosphate in soils [12]. A recent review by Brimmer, Griffiths and Harrick states that numerous commercial diffuse reflectance accessories have been developed to fit in the compartment of FT-IR spectrometers (Harrick Scientific, Barnes-Spectrotech, Specac, Analet Instruments, JASCO International and Mattson Instruments) [13]. Harrick Scientific Corp. produced a vacuum chamber, HVC-DRP, which provided the impetus for this research. The chamber is isolated from the spectro-meter. Only the radiation which is transmitted through the KBr windows is exchanged with the spectrometer. The atmosphere (or vacuum) above the sample and The temperature of the sample are controlled by the operator.

1.2 Objectives

The purpose of this research is threefold. First, the theory of diffuse reflection from a powder surface was studied to determine any

theoreticai limitations. Answers to the foilowing questions were sought. Can an undiluted or neat sample be used? What restrictions exist for using a neat sample? In order to understand the theory of diffuse reflection, many other phenomena associated with the interaction of eiectromagnetic radiation and matter needed to be understood. There have been several solutions given to the probiem of specuiar refiection when conducting diffuse refiection spectroscoy, but most of these have faiied to address the more generai problem of coherent scattering. Since the same terms are used differentiy by different authors, the terminology and accompanying mechanisms needed to be understood before proceeding to the other theoretical questions.

Second, the IBM Fourier transform spectrometer and the DRIFT praying mantis accessory needed modification for use with the Harrick in-situ DRIFT cbamber. Daimay L. Vein, a graduate chemistry student, provided invaiuble assistance in designing the necessary modifications. Upon completion, the equipment wouid have been checked out, but a cooling line in the spectrometer burst. The spectrometer was rendered unuseabie by the water damage. Therefore, each component of the ceii and tbe various modifications have been checked separateiy, but have not been used on the FT-IR spectrometer. The experiments which would have been conducted are included in Chapter 7, Conciusions and Recommendations, as recommendations for future work.

Third, the surface of aiumina was to have been studied using DRIFT. The dehydroxyiation of bayerite and boehmite to η-aiumina and γ-aiumina wouid have been conducted. Bayerite and boehmite were prepared using an amaigamated procedure. The iow temperature aluminas were heated to 550°

to 600°C, eliminating water. The dehydroxylation was accompanied by a phase transition to η- and γ-alumina, respectively. The dehydroxylation was not performed in the in-situ chamber, because of the damaged spectrometer. Each alumina phase was verified with x-ray diffraction.

A fourth objective was added when a near-IR diffuse reflectance Fourier transform spectrometer became available. The hydroxyl bands of bayerite, boehmite, γ-alumina and α-alumina were examined to determine the usefulness of the near-IR region in the study of catalysts. The same samples were used in both the near-IR and mid-IR spectra.

1.3 Definitions

1.3-1 *Absorption*: During absorption, there is an inelastic transfer of energy between an electomagnetic field and matter. Usage in this paper will be confined to those situations where the atom is excited from one characterstic energy level to another by the direct adsorption of a quanta of energy.

1.3-2 *Resonant Emission*: Resonant emission is the reverse process of absorption and is characterized by the emission of a photon as the molecule relaxes to a lower quantum state. The two special types of resonant emission, flourescence and phosphorescence, are differentiated by a change in spin multiplicity in the molecule. For *flourescence*, the molecule does not change spin multiplicity and remains in the singlet state throughout the absorption emission process. There is some emissionless relaxation prior to the radiation of a photon and relaxation to

a lower energy level. Therefore, the wavelength of the radiation emitted during flourescence is always longer than that wavelength originally absorbed [14]. During *phosphorescence* the molecule changes spin multiplicity during the relaxation and emission of a photon. The excited molecule first undergoes an intersystem crossing from a singlet state to a triplet state. After a radiationless relaxation to the lowest triplet state, it relaxes to a lower singlet state, radiating a photon (see figure 1). Phosphorescence is a slower process and secondary radiation persists even after all of the incident radiation has been stopped.

1.3-3 *Scattering*: Scattering is defined as an interaction between radiation and matter which changes the direction of the incident radiation. It is a nonresonant phenomena involving the excitation of the atom to a virtual state rapidly followed by a reemission of a photon and return to the original energy level. The virtual state is a function of the energy of the incident EM field. Since this energy level does not correspond to a characteristic energy level of the atom, it is not stable. The Heisenberg uncertainty principle can be used to predict the time constant for this "excited state":

$$\Delta E \Delta t = h/2\pi \quad [16] \qquad (1)$$

where h = Plancks constant and ΔE=energy of absorption level minus the

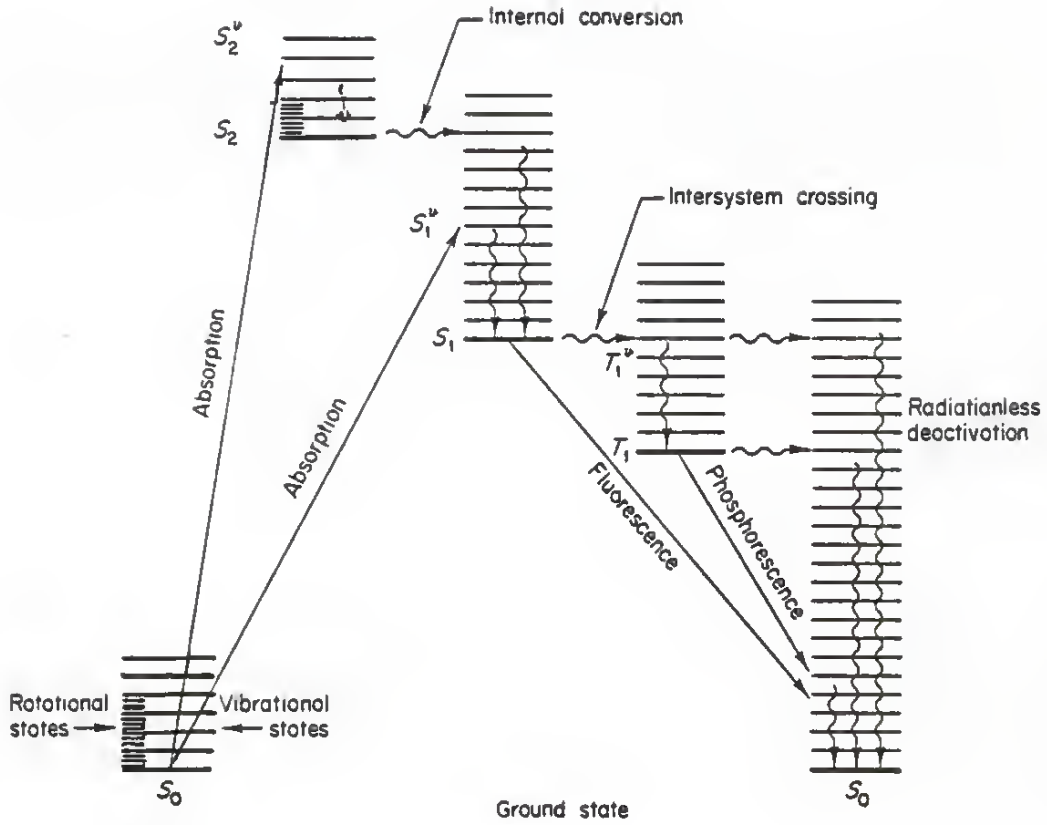

Figure 1. Various photophysical processes. Radiative transitions are given by solid lines while radiationless transitions are given by wavy lines. S_0, S_1 and S_2 are electronic states. Rotational and vibrational states are indicated with fine structure [15].

energy of incident radiation. The virtuai state is transient, on the order of 10^{-8} to 10^{-12}seconds [17], with the atom reiaxing instantaneously and reradiating the energy. In this way, a portion of the incident EM field is scattered off the atom (see figure 2).

Scattering is nearly elastic, as radiation is transferred to the atom and then reradiated out in any direction. Different names have been given to the types of scattering based on the reiative particle size, the waveiength of the incident eiectromagnetic radiation and the polarizabiiity of the moiecules. The term *Mie scattering* is used for scattering from isotropic sphericai particles of any size [18]. The radiation is scattered through greater angies for the shorter wavelengths. In the case of *Rayleigh scattering*, the particles are smaii compared to the wavelength of the iight and are randomiy distributed throughout the medium. Shorter waveiength iight is scattered more intenseiy. Specifically, the intensity of the scattered iight is proportional to λ^{-4}. The earth's atmosphere provides an excelient exampie of Rayieigh scattering. Since biue iight posseses the shortest waveiength in the visible range of the spectrum, it is scattered more intenseiy by tbe atmosphere. At dusk or dawn, light must pass a long distance through the atmospbere before it reaches an observer, hence oniy the ionger red waveiengths are stiii present. When the radii are of the same order of magnitude as λ, and the particles are uniformly spaced, scattered iight will constructiveiy interfere from one particle to the next. The resuitant scattering pattern wiil be marked by discrete bands and is cailed *diffraction*.

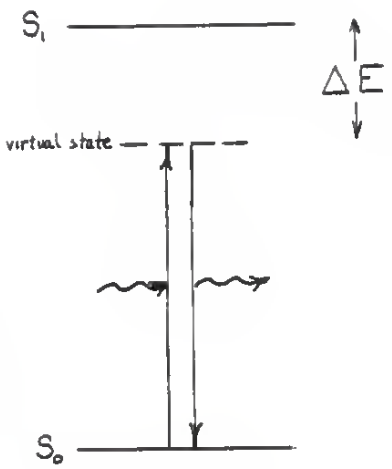

Figure 2. Scattering process. The incident EM field does not possess an energy level corresponding to a characteristic frequency. The time constant for the process is inversely proportional to ΔE. The frequency of light scattered is the same as the incident EM field.

1.3-4 Raman scattering: In some cases, the molecules undergo induced polarizability as a result of the electric field. "If the polarizability oscillates because of rotation and vibration of the molecules to which tbe electrons are bound, the scattered light will be amplitude modulated." [19]. When this happens, the scattered light possesses a higher or lower frequency than the incident light. The change in frequency is equal to the energy transfered to the molecule, which has undergone a vibrational-rotational transition. This is called *Raman Scattering*. During Stokes scattering, the atom is excited to a virtual state followed by an instantaneous relaxation to an excited energy state. Stokes scattering is about a thousand times less intense than the accompanying Rayleigh scattering. Likewise, anti-Stokes scattering applies to Raman scattering is excited from a energetic state to a virtual state and then relaxes to the ground state. (see figure 3).

1.3-5 *Transmission*: Transmission, as it applies to spectroscopy, refers to the passing of radiation directly through the sample. Radiation will be attenuated through scattering, reflection, and absorption. When transmission occurs through homogeneous media with uniform spacing, the scattering patterns from each atom constructively interfere. Little radiation is lost as a result of this constructive scattering, but the phase is delayed giving a slower transmission velocity. This phenomenon is defined as refraction [21].

1.3-6 *Reflection*: Reflection of light is a multifaceted phenomena. First, there are two distinct limiting cases, diffuse reflection and

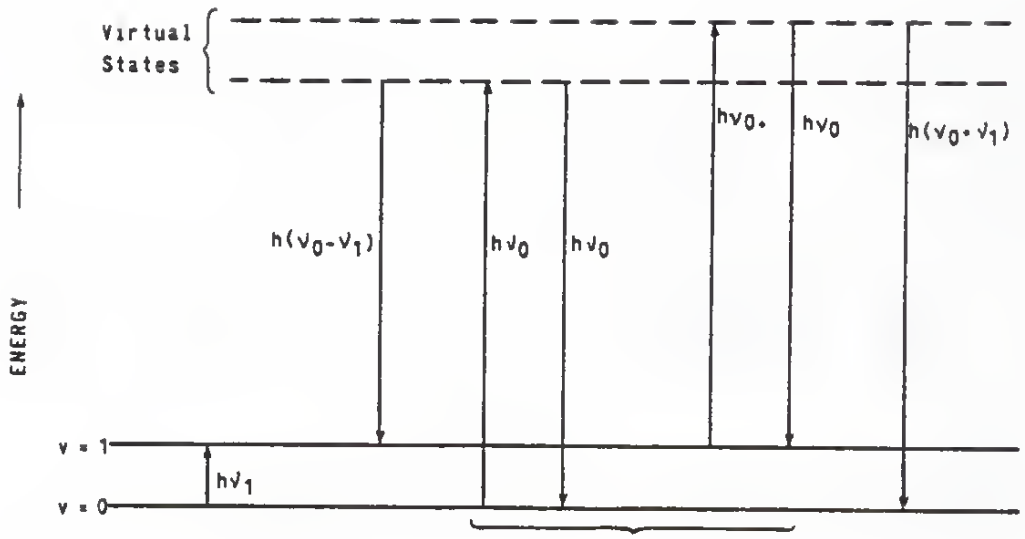

Figure 3. Raman scattering diagram. This energy level diagram illustrates the fundamental processes of Raman scattering. The incident EM field is of energy h_{ν}. Raman bands appear at $h(\nu_o - \nu_1)$, Stokes scattering, and $h(\nu_o + \nu_1)$, anti-Stokes scattering [20].

specular, or regular, reflection. Regular reflection is that reflection where the angle of the incident light equals the angle of the reflected light. This is best characterized by the reflection from a smooth metallic surface. Regular reflection is coherent scattering caused by phase related oscillations of adjacent atoms or particles. The terms specular reflection and diffuse Freshnel reflection were chosen based on a paper by Brimmer et. al. [13]. The article used the term Kubelka-Munk reflection for the reflection which has been transmitted through the particles. However, basing the definitions for the two types of diffuse reflection on whether the radiation is transmitted through the particles or not is inappropriate. It fails to address the complicated nature of scattering from a powder in which the particles are on the same order of magnitude as the wavelength of the radiation. Therefore, the term, Kubelka-Munk reflection, is excluded from this paper.

1.3-7 *Specular reflection*: Specular reflection will only be used for reflection from the overall surface, that is "mirror" reflection from the plane of the sample. The specular angle is defined by the angle of incidence with respect to the surface of the powder as a whole. The relative intensity of specular reflection is greater for larger angles of incidence.

1.3-8 *Diffuse reflection*: Diffuse reflection is that reflection which is radiated off in all directions and is best characterized by the reflection of visible light from a white surface (flat texture). From a powder, diffuse reflection can arise in two different ways. It is

necessary to differentiate between them. The term, diffuse reflection, will apply only to reflection that is a result of isotropic scattering. This is a bulk phenomena and is the result of a combination of multiple scattering and reflection, refraction and diffraction.

1.3-9 *Freshnel diffuse reflection*: Diffuse Freshnel reflection, on the other hand, is the result of regular reflection at the particle surfaces. The radiation is not transmitted through the individual particles as is generally assumed for diffuse reflection. Freshnel diffuse reflection is coherent and violates the theoretical treatment for diffuse reflection.

No surface exhibits pure specular reflection. Likewise no surface exhibits pure diffuse reflection nor pure diffuse Freshnel reflection. Rather reflection is the superposition of these different types of reflection.

Chapter 2

Spectroscopy

Several different detection techniques are used in the infrared region of the spectrum (see Table 1). Transmission IR is by far the most widely used technique. Haller cautions "None of these spectroscopies (other techniques) are recommended if the question asked can be answered using conventional transmission spectroscopy." [3] With this guiding thought, the limitations of transmission IR and subsequently the benefits and limitations of diffuse reflectance infrared Fourier transform (DRIFT) spectroscopy will be examined in detail.

TABLE 1

Vibrational Spectroscopic Techniques

I. Photon vibrational spectroscopies
A. Transmission-absorption infrared
B. Reflection-absorption infrared
a. Internal reflection
b. Specular reflection
c. Diffuse reflection (DRIFT)
C. Raman scattering
D. Emission
E. Infrared absorption calorimetry
a. Direct calorimetry
b. Photoacoustic (PAS)
II. Electron vibrational spectroscopy
A. Electron energy loss (EEL)
B. Inelastic electron tunneling
III. Inelastic neutron scattering spectroscopy

[3]

2.1 *Transmission IR*

In transmission spectroscopy the sample is irradiated and the radiation that passes through the sample is measured. The intensity of the transmitted radiation is divided by that of the incident beam. The results are plotted as a percentage transmission. Radiation is lost in three ways. First, it will be specularly reflected at the surface. The amount can be determined by using the Freshnel equations and will be examined later. In general, it will be of the order of 4%, but increases significantly for strong absorption bands. Second, radiation will be lost through scattering because of inhomogeneities. It is essential that the particles be smaller than the shortest wavelength used to minimize these losses. Making the particles sizes this small through grinding is extremely difficult for very hard, inorganic samples such as alumina. Finally, radiation will be lost from the incident beam by absorption. Ideally, only absorption losses would occur. The energy balance for the intensity of the transmitted radiation is:

$$T = I_o - S - R - A \qquad (2)$$

where I_o=incident radiation, S=scattering, A=absorption and R=specular reflection. In most discussions, losses due to specular reflection are included as part of the scattering. In this paper, specular reflection has been separated from the scattering to provide a uniform procedure for handling specular reflection in both transmission IR and DRIFT.

Various sample preparation methods are used for transmission IR.

It is well known that different preparation methods can produce somewhat different spectra [22]. The use of an undiluted powder sample was one of the early procedures for conducting infrared spectroscopy with solids. There is excessive scattering when an undiluted, uncompressed powder is used in transmission IR. This has also been utilized recently for studying adsorbed species [23,24]. It has been accomplished by placing a fine powder sample between two windows and then irradiating it. The species being adsorbed is then passed between the windows.

The best, or truest, absorption spectra is produced by suspending the sample in a mineral oil, such as NUJOL or flourolube, to form a mull [22]. One problem with using mulls for irradiating inorganics is the Christenson effect [22,25]. This can occur when the index of refraction of the matrix matches that of the sample. The net result is enhanced transmission, giving rise to a spurious absorption peak [25]. The phenomena is often observed in a region of anomalous dispersion, where the refractive index decreases sharply in strongly absorbing species. Additionally, the absorption bands of the mineral oil can interfere with the absorption bonds of the sample. By taking spectra with two different mineral oils, an area that is obscurred in one mull will be visible in the other. It is virtually impossible to get the same sample concentration in each mull. This reflects a general difficulty in obtaining quantitatively reproduceable spectra. The quality of a mull is a function of the thickness of the layer pressed between the two windows. If the particles are too large, a thin layer cannot be made and the transmission is exceptionally poor. Finally, the sample is

inaccessible to adsorption or desorption from the gas phase once it has been made into a muii.

The other standard procedure is to disperse the sample in a nonabsorbing matrix, such as KBr, and press it into a disk (15000-20000 psi). This method is more difficult to accomplish than the mull, but it provides greater control over the concentration of the sampie. KBr is transparent in the mid-infrared region of the spectrum so there are no extraneous absorption bands from the matrix. Since the Christensen effect is observed when the refractive index of the matrix approximateiy equals the sample, it is aiso a potentiai problem when using the KBr pressed disk method. The scattering iosses with a KBr/sampie window are dependent on the quaiity of the window. Making these windows is an art, requiring practice and patience. Inorganic sampies can undergo ion exchange with the matrix, changing the spectra, as shown in the work of Iwaoka et al. (see figure 4) [22]. Furthermore, the sampie is inacesibie to adsorption or desorption studies once it has been pressed into a KBr peilet.

At times, a neat sampie has been pressed into a seif supporting disk or wafer. The sample is piaced in a die and pressed under 15,000 to 20,000 PSI into a seif supporting disk. Peri reports that this is a satisfactory approach, but can be quite troublesome [23]. Severai hours were spent unsuccessfuiiy trying to make a suitable aiumina disk. The disks cracked and crumbied easiiy because the alumina stuck to the die under the applied pressure. A die with a smaii boit at either end was used for each pressed disk in this research (see figure 5). The other sampie dies which were availabie required that the wafer be removed from

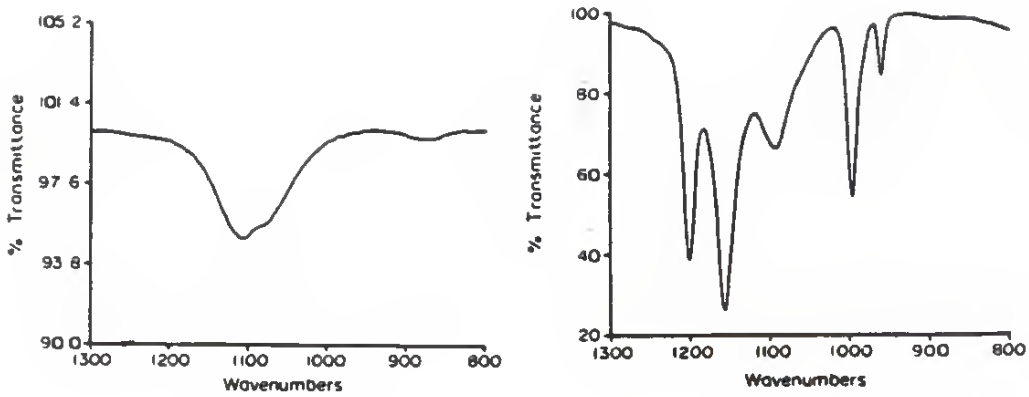

Figure 4. Specular distortion with a KBr pressed wafer. This figure is the transmittance spectra of $CuSO_4 \cdot 5H_2O$ prepared as a KBr disk (right) and as a NUJOL mull (left). The spectra from a NUJOL mull is more representative of the true absorption spectra than a KBr wafer [10].

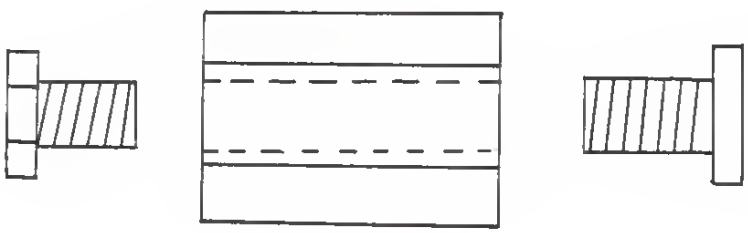

Figure 5. Transmission wafer die. The powder sample is compressed into a thin transparent wafer with this die. The sample is placed in the die after the first nut is tightened. The second nut is then tightened to compress the sample into a wafer.

the die before being used. If self supporting wafers are used, the die should be designed such that the pressure is applied vertically without torque. Secondly, the wafer should be in a die which can be set directly in the spectrometer. Unless unusually high pressures are used supported wafers will retain most of their original surface area [23]. These undiluted wafers transmit poorly, because of the thickness required to make a self-supporting wafer [23]. The diffusional resistance for adsorption of a gaseous phase will certainly be increased as the powder is pressed into a wafer.

Finally, a thin film of sample can be deposited on a alkyl balide window. Use of deposited sols is generally limited by the sample preparation requirements. Minor deviations in the procedure may lead to varied properties in the sample or to unsatisfactory plates. In Peri's research on γ-alumina, the sols were made as aerogel plates taking in excess of 2 weeks [26]. His aerogel plates had a surface area of about 300 m^2/g and were 90% transparent from 4000 cm^{-1} to 1890 cm^{-1}. Below 1900 cm^{-1}, absorption from the alumina lattice severely attenuated the transmission, which fell to 23% at 1300 cm^{-1} [27]. Additionally, severe scattering from non-uniformities or graininess can be a problem with this technique.

It would be helpful if the spectra could be taken from a powder sample. This would eliminate the special preparation and enhance the ability to examine the surface. The sample could be examined under conditions more closely approximating those being modeled. The use of a powder sample in transmission IR is severely limited by scattering.

Other techniques have been sought that would permit analysis of undiluted or untreated samples. Emission IR and photoacouatic methods use powder samples. In DRIFT the powdered sample is normally mixed with a finely ground nonabsorbing matrix, but it can be studied as a neat sample.

2.2 *Emission IR*

In emission IR, the sample is heated and the emitted radiation is measured as a function of wavelength. From Kirchoff's law, the absorptivity can be equated to tbe emissivity at any temperature for a solid in equilibrium [28]. It can also be shown that the two are equal for each wavelength separately:

$$e_\nu = a_\nu \tag{3}$$

where e_ν= emissivity wavelength and a_ν= absorptivity wavelength.

The major problem in conducting emission IR is the temperature gradients that exist across the sample. Not only are many catalysts poor conductors, they often are in powdered form whicb further reduces their conductivity. The resulting gradients are quite extreme. In calibrating the variable temperature Harrick in-situ DRIFT chamber, the surface temperature of the $K_2Cr_2O_7$ sample was found to be about 100°C less than the base of the cup (a distance of 3 mm). It should be noted that the KBr windows were not used and therefore both convection and conduction of heat were significant. The transfer of heat from the

sample was significantly greater than would be experienced under vacuum conditions. Sample decomposition has been identified as another problem with emission IR. Except under extreme conditions, this should not affect the catalytic samples of interest. For these reasons, good quantitative measurements by emission IR are very limited [29].

2.3 *Photoacoustic IR Spectroscopy (PAS)*

In photoacoustic IR, the sample is placed in a closed environment with an inert gas and a microphone. The sample is irradiated by a laser or a broad infrared source. When a characteristic frequency of light is absorbed by the sample, the sample is heated. The heated sample generates a modulated temperature fluctuation at the same frequency as the incident radiation (but not necessarily with the same phase) [30]. The emitted radiation heats the gas next to the sample which expands and sets up a pressure wave which is detected by an acoustic microphone. The gas must not absorb any of the incident radiation.

2.4 *Diffuse Reflectance Infrared Fourier Transform Spectroscopy*

In DRIFT spectroscopy, the powdered sample is irradiated and the reflected radiation is collected and measured by a detector. The two most common detectors are mercury cadmium telluride (MCT) and deuterated triglycine sulfate (DTGS) with MCT being the most sensitive. Since the collecting mirrors only encompass a portion of the hemisphere above the sample area, not all of the reflected radiation will be collected (see figure 6). Furthermore, the specular and diffuse components are superimposed. Therefore, diffuse reflectance cannot be measured

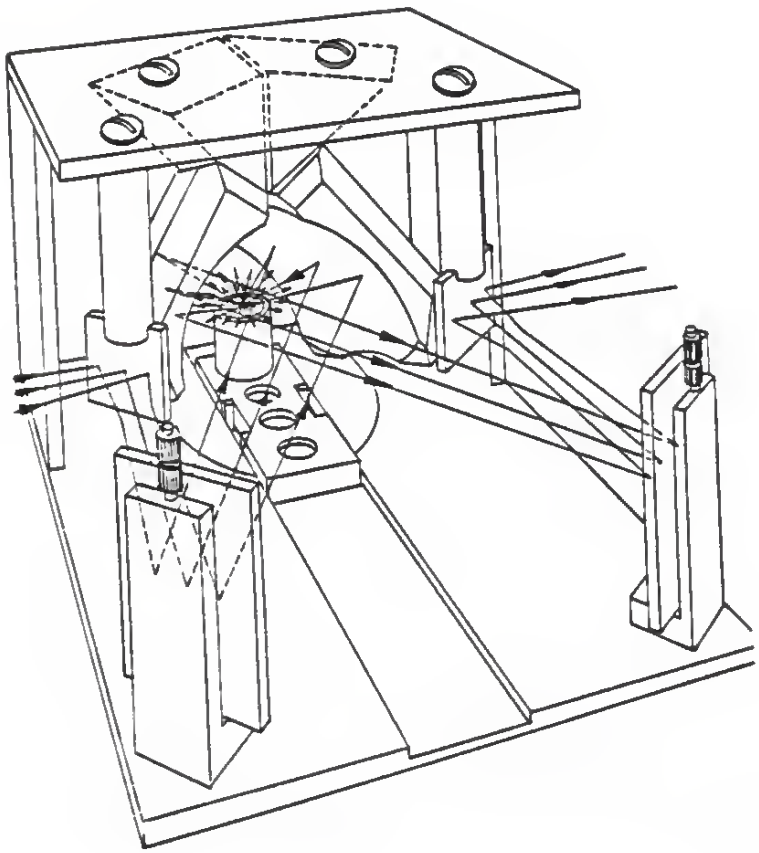

Figure 6. Praying mantis accessory for diffuse reflectance spectrometry. The design incorporates ellipsoidal focusing and collection mirrors and fits into the sample compartment of commercial FT-IR spectrometers [30].

directly. The reflection of the sample is set as a ratio against the reflection from a nonabsorbing reference material, such as KBr or KCl. The energy balance for the total reflection from the sample is:

$$\text{Reflection} = R_D + R_{DF} + R_S = 1_0 - A \qquad (4)$$

where R_S= specular reflection and R_D= diffuse reflection and R_{DF}=diffuse Freshnel reflection. The coherent scattering effects, specular and Freshnel diffuse, need to be seperated or eliminated from the "true" diffuse reflection. When there is little coherent scattering present in the reflection, the resulting spectra shows the same absorption bands as transmission IR, albeit with different relative intensities.

2.4-1 DRIFT Praying Mantis Accessory

The Harrick Praying Mantis DRIFT accessory is one configuration for a DRIFT accessory. It fits into the sample compartment of standard commercial spectrometers (figure 6). The sample chamber lies between the interferometer and the detector. With this accessory, the radiation is directed from the mirror on one side to the sample area and then is collected by the mirror on the other side (both mirrors are elliptical). In its simplist configuration, it collects all of the specular component and some of the diffuse components. Adjustments can be made to eliminate the specular component [30], but are not needed when the controlled atmosphere cell is used. The inlet and exit beams are in different planes due to the location of the windows. This alignment

precludes the specular component from exiting the cell and being collected. Other DRIFT accessories are available, but will not be reviewed in this paper. Griffith and Haseth have a section in their book on FT-IR that reviews several of the accessories [30].

Since specular reflection is a key issue, some of the methods for eliminating it will be addressed. Fuller and Hamadeh have constucted DRIFT accessories in which the incident beam impinges the sample area perpendicularly [8,31]. With this configuration the angle of incidence equals the angle of regular reflection. Therefore, the specularly reflected light islost through the same hole in the mirror that the incident beam travels through; ie. at 0^{o}. Spectrotech designed a specular blocker for their DRIFT accessory that can be lowered into the sample area, to block specular reflection [32]. Clearly, the specular component of reflection can be eliminated.

However, that does not completely solve the problem with regular reflection. Coherent scattering is the cause of regular reflection, which occurs at the surface of a crystal, metal face, mirror, etc. With a powder, the crystal surfaces have various orientations and can regularly reflect radiation in all directions, ie. appear as diffuse reflection. Regular reflection is strongly affected by absorption bands, as will be shown in section. Both specular and Freshnel diffuse reflection are affected by particle size.

Kortüm discusses two approaches that may be used for reflectance spectroscopy to measure diffuse reflection. In both methods the sample is ground to fine particles; ie., on the order of the wavelength used.

In the first approach, the sample is diluted to about 1% concentration with a finely ground nonabsorbing matrix. This isolates the sample particles from one another. In general, the scattering properties of the dilute mixture are determined solely by the matrix material. As the concentration of the sample tends toward zero this method rigoroualy obeys the Kubelka-Munk equation and provides good quantitative results [18,33]. As the concentration of the sample tends to zero there is very little sample present. For the study of surfaces, the adsorbed species is the spectral group of interest. It's concentration may be exceedingly low. Another drawback to the dilution method involves hydroxylation experiments. KBr and KCl both adsorb water strongly, thereby interfering with the reaction being studied. There may be other instances where the matrix adsorbs either the reactant or the products. This constitutes the biggest complaint with the matrix method.

In the second method, a neat sample is irradiated. Crossed polarizers are utilized to discriminate against regular reflection. Diffuse reflection will be unpolarized whereas any radiation that has undergone a single regular reflection will be polarized. The incident beam is linearly polarized by the first polarizer. The second polarizer is rotated 90° and placed between the sample and the detector. This method will eliminate the specular component and much of the diffuse Freshnal component. The radiation that is still polarized will be blocked. Additionally, half of the unpolarized radiation will also be blocked at this second polarizer. This method will not distinguish between multiply reflected diffuse Freshnel and true diffuse reflection. This technique has been used in the visible and uv regions, but has not

been used in the infrared region of the spectrum. The intensity of radiation available is severely limited, even in the visible region of the spectrum [18].

2.4-2 Quantitative DRIFT Spectroscopy

Since there is not a rigorous theory for multiple scattering, many have attempted to develop a phenomenlogical theory for scattering [18]. Several different approaches have been used. Continuum models bave proven more effective than discrete models. Discrete models are appropriate when the particles are considerably larger than the wavelength of tbe incident radiation, the interactioos can still be conceived in terms of reflection, refraction and diffraction.

Schuster was the first to solve the radiative transfer equation. He simplified the radiation field into two oppositely directed radiation fluxes [18,34]. Chandrasekhar's book covers many rigorous soluitons of the equation [35]. Several others solved the equation for specific applications [38,37,38]. Kubelka and Munk chose to use a simplified approach and address the problem by considering tbe absorption and scattering that takes place tbrough a differetial layer [39,40]. They arrived at the same solution as Scbuster. The Kubeka-Munk equation is a two parameter model.

2.4-2a *Kubelka-Munk Equations*

The Kubelka-Munk, or Kubelka-Munk-Schuster, equation is the most general and most widely accepted quantitative relationship for DRIFT. One spectroscopist stated that neither he nor others used the Kubelka-Munk function to treat data, because it erroneously assigned values in

excess of 100% transmission. His comments served as a reminder that many theoretical tools are applied without the requisite understanding of their limitations. Therefore, the derivation of tbe Kubelka-Munk equation is provided below. It is an extract of the derivation found in Kortüm's book [18]. It is necessary to make certain simplifying assumptions in the development of the Kubelka-Munk equation. The assumptions are:

1) The Lambert Cosine law is valid (isotropic distribution of scattering) so that any regular reflection is neglected.

2) The particles in the layer are randomly distributed and very much smaller tban a layer (continuous media assumption).

3) The layer is subject to diffuse irradiation (inverse concept of diffuse reflection).

Two oppositely directed radiative fluxes are defined. Either the radiation is penetrating deeper into the sample (radiation flux I) or it is being remitted toward the surface (radiation flux J) (see figure 7).

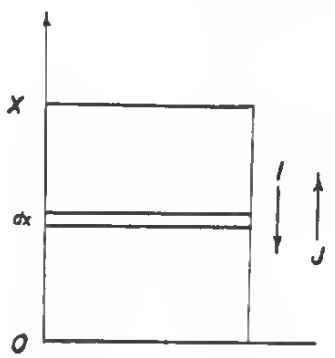

Figure 7. I and J fluxes. This is a diagram depicting the radiation fluxes for irradiation of a sample according to the Kubelka-Munk Theory.

The energy lost during absorption or scattering is considered to be constant with respect to the distance traveled, $d\xi$; ie., directly proportional to the path length. The mean free path is calculated by integrating over the angular distribution of the radiation, assuming diffuse irradiation of each layer. Kortüm showed that the mean free path length through a layer is twice the thickness of that layer, $d\xi_I = d\xi_J = 2dx$, for diffuse, incident radiation . Additionally, if parallel incident radiation at $\Theta = 60°$ is used, the mean free path is still twice the distance through a layer, since the cos (60°)=0.5. The development of the Kubelka-Munk equation is still valid. The isotropic scattering within each "layer" produces diffuse incident radiation for the next "layer". The radiation is only transmitted a small depth before it becomes diffuse. The differential equations for the change of energy for each flux with respect to the positive x direction are:

$$-dI = -kI(2dx) - sI(2dx) + sJ(2dx) \qquad (5)$$

and

$$-dJ = -kJ(2dx) - sJ(2dx) + sI(2dx) \qquad (6)$$

where k = absorption coefficient and s=scattering coefficient (both defined in terms of the radiation lost per distance traveled). These equations can be simplified by letting K=2k, S=2s, and $a = \frac{S+K}{S}$. Tbe equations reduce to:

$$-\frac{dI}{Sdx} = -aI + J \qquad \text{and} \qquad \frac{dI}{Sdx} = -aJ + I \qquad (7)$$

These two equations may be combined by dividing the first by I, the second by J and using the tranformation r = J/I, giving:

$$\frac{dr}{Sdx} = r^2 - 2ar + 1 \qquad (8)$$

The following boundary conditions apply:

for x=0; $(J/I)_{X=0} = R_G$ reflectance of background

for x=d; $(J/I)_{X=d} = R$ reflectance of the sample

for the case where d=∞, R_G=0, and the reflectance is:

$$R_\infty = \frac{S}{S + K \cdot (K(K+S))^{1/2}} \qquad (9)$$

where R_∞ = reflectance from an "infinitely" deep sample. At first appearance, this might appear to be a stringent assumption. In the IR region of the spectrum it has been shown that an infinite deptb is achieved at less than 3 mm. The penetration is significantly less for absorbing materials. The KM equation is more commonly expressed in terms of K/S as follows:

$$K/S = F(R_\infty) = \frac{(1- R_\infty)^2}{2 \cdot R_\infty} = \frac{2.303 \cdot a \cdot c}{s} \qquad (10)$$

where a=absorption coefficient and c=concentration. As the concentration of the absorbing sample in the matrix is decreased, R_∞ tends to unity, so that:

$$(1-R_\infty) = \left(\frac{4.605 \cdot a \cdot c}{s}\right)^{\frac{1}{2}} \qquad (11)$$

The signal-to-noise ratio (SNR) is proportional to the square root of the concentration of the sample. The concentration is proportional to the abaorbance according to the Lambert-Beers law, however, for transmission spectroscopy. Therefore the SNR for DRIFT spectroscopy will be much than tbe SNR for transmission spectroscopy as the concentration tends to zero. DRIFT spectroscopy is suited well for microaampling. For example, while taking the spectra in this research, adsorbed CO_2 was clearly visible in the DRIFT spectra of γ-alumina, but scarcely visible in the transmission spectra (in Chapter 6).

2.4-2b *Pitts-Giovanelli and Rozenberg Formulas*

In practice, the Kubelka-Munk function is linear in concentration over a very limited concentration range. The underlying theory breaks down when coherent scattering from the absorbing sample becomes a factor. Hecht has compared the Kubelka-Munk function with other predictive equations for five different media. Two of the mediums are of

psrticular interest. The first is for s two component system in which one component is an intense absorbent and the other component is a nonabsorbing scatterer [41]. The Pitts-Giovanelli formula provides the best fit, but the formula does not always converge. The Rozenberg formula is very stable snd provides a moderately good fit.

The second medium of interest was for cases in which the absorber is absorbed on the surface of the scsttering particles. Hecht used resorcinol blue in ethsnol to prepsre solutions of varying concentrations which were combined with alumina (no phase identified) [35]. The Kubelka-Munk function was generally linesr in concentration over spproximately 4 orders of magnitude. Pitts-Giovanelli snslysis provided little improvement over the Kubelka-Munk equation.

The Pitts-Giovanelli formula was derived from the rsdiative transfer equation [37,38]. Anisotropic scattering is accounted for in the phase function used with the rsdiative transfer equation. Only one additional parameter, x, is used with the Pitts-Giovanelli formula as compared to the Kubelka-Munk equation. This parameter, x, is a measure of the snisotropy of scatter. The Pitts-Giovanelli formula is an excellent spproximation to the complete solution of the radiative transfer equation for all values of x for which solutions exist [36]. A msjor disadvantsge to its use is the sensitivity that it experiences with respect to the choice of initial parameter values. The equation fails to converge in some cases. This formula provided the best fit for each system that Hecht studied which possessed significsnt anisotropic scattering.

The Rozenberg formula, on the other hand, relates the observed reflectance to the ratio of absorption and scattering coefficients. A power series expansion is used. For mediums which absorb appreciably, the attenuation of radiation is rapid and only the low order terms are retained. The Rozenberg formula yields moderately good fit and is very stable. Hecht preferred the Rozenberg formula or the Kubelka-Munk theory to Pitts-Giovenelli because the Pitts-Giovanelli formula had often failed to converge.

The Pitts-Giovanelli and Rozenberg approaches are capable of of satisfactory results for greater sample concentrations than the Kubelka-Munk theory. Each of these formulas is still only capable of treating dilute samples, however. The quantitative treatment for the multiple scattering of radiation for closely spaced absorbing particles is probably not possible. The processes are too complex when the absorbing particles are of the order of the wavelength in size and closely packed.

The coherent scattering effects must be minimal to conduct quantitative analysis. One method is to dilute the sample witb an inert matrix. KBr and KCl are not good choices for inorganic compounds. Both can undergo ion exchange with the sample during the grinding and mixing steps of tbe sample preparation. Both are also hygroscopic and therefore interfere with the hydroxyl region of the spectrum. Silicon may prove to be acceptable, but it still needs to be tested quantitatively. The use of cross polarizers will isolate and eliminate most of the coherent scattering. Unfortunately, the intensity of the radiation

available in the mid-IR region of the spectrum is minimal posing a major constraint to the use of cross polarizers.

Chapter 3

The interaction of radiation with matter

Numerous sources have identified specular reflection as a major problem when using DRIFT to study strongly absorbing materials. As discussed in chapter 2, various schemes have been devised to cope with specular reflection. These schemes only solve one aspect of the coherent scattering problem. The mechanism for coherent scattering must be understood. Its relationship with particle size and dispersion will follow. Restrahlen bands will also be discussed in this chapter.

3.1 Classical analysis of the interaction of electromagnetic (EM) radiation with dielectric solids

When a dielectric is subjected to an incident electric field, the internal charge distribution distorts under its influence. The electron cloud of each atom shifts relative to the nucleus, producing a dipole moment. The electric polarization, P, is proportional to the applied field, E, for most materials [42]. Since the incident electromagnetic (EM) field is periodic, the polarization of the dipole moments of the dielectric will also oscillate. The oscillations of the atom's electron charges is the subject of this section.

The analytical treatment of radiation and matter is the domain of quantum mechanics. The classical treatment, however, leads to very similar results and provides an excellent conceptual model [21,42]. In the classical treatment, the atom is modeled as an oscillator being driven by a periodic force. The force that is felt by an electron of

charge q_e by the an EM field, E(t), is $q_e E_o \cdot \cos(\omega \cdot t)$. The valence electrons are bound to their respective atoms by a restoring force $(m_e \omega_o^2 \cdot x)$ which is proportional to its displacement, x. The differential equation is therefore:

$$m_e \frac{d^2x}{dt^2} + m_e \omega_o^2 x = q_e E_o \cdot \cos(\omega t) \qquad (12)$$

The solution for this differential equation is:

$$x = {q_e E_o \cdot \cos(\omega \cdot t)}/{m_e(\omega_o^2 - \omega^2)} = {q_e E(t)}/{m_e(\omega_o^2 - \omega^2)} \qquad (13)$$

The charge will oscillate at the same frequency as that of the incident EM field. Each charge in the electron cloud will experience the EM field and will, therefore, oscillate at the same frequency, producing an oscillating dipole. An oscillating dipole will radiate its own EM field. This concept will be reintroduced later.

In solids, the atoms cannot be considered as isolated oscillators because of their close proximity to other atoms. Strong mutual interactions exist between the atoms resulting in "frictional" force. This force damps the oscillations, dissipating energy within the dielectric in the form of heat (molecular motion) [42]. The damping force is proportional to the velocity of oscillator, $\gamma \frac{dx}{dt}$. Incorporating the damping force into the differential equation gives the following solution:

$$x = {q_e E(t)}/{m_e(\omega_o^2 - \omega^2 + i \cdot \gamma \cdot \omega)} \qquad (14)$$

Generally, $(\omega_o^2-\omega^2) >> i\cdot\gamma\cdot\omega$ and no significant dissipation of energy takes place. When ω approaches ω_o, the absorption frequency, the intensity of the oscillations will increase dramatically. The equation predicts, as expected, that the absorption of energy at this frequency will be significant. It also predicts a complex component of the displacement, which significantly alters the refraction and reflection of the material.

It can be shown that the refractive index for N oscillators possessing j characteristic frequencies is [41]:

$$\frac{n^2-1}{n^2+2} = \frac{N_{qe}^{\ 2}}{3\cdot\epsilon_o m_e} \sum_{j=1}^{N} \frac{f_j}{\omega_{oj}^2 - \omega^2 + i\cdot\gamma\cdot\omega} \qquad (15)$$

where f_j is the transition probability of a particular transition and ϵ_o is the electric permittivity of free space. As ω^2 is increased toward ω_o^2, $(\omega_{oj}^2 - \omega^2)$ decreases and n gradually increases. When $\omega^2 \approx \omega_{oj}^2$, the denominator becomes small and the complex component dominates. The index of refraction n increases rapidly and is complex. As ω continues to increase at frequencies higher than ω_{oj} the refractive index decreases. When the refractive index decreases as the wavelength increases, this is defined as anomolous dispersion. When the index of refraction increases and becomes complex, it significantly increases the specular reflection. This will be examined in section 3.3.

3.2 The Dielectric Constant and the Forbidden Frequency Zone

A more detailed approach to the propagation of radiation through crystals is provided through solid state physics. The propagation of an elastic wave through a crystal is quantized. The quantum of energy in a lattice vibration is called a phonon, analogous to a photon in an electromagnetic wave. Kittel discusses the response of a diatomic lattice to infrared photons [43]. He showed that the frequency dependent dielectric constant, $\epsilon(\omega)$, equaled:

$$\epsilon(\omega) = \epsilon(\infty) + \frac{S}{\omega_T^2 - \omega^2} \qquad (16)$$

where $\epsilon(\infty)$ denotes the core electron contribution, ω_T = resonant frequency, and S is a constant. A plot of equation 16 is shown for arbitrary values of $\epsilon(\infty)$ & S/ω_T^2 (see figure 8). Electromagnetic waves will not propogate in an infinite crystal in the forbidden frequency region.

$$\omega_T^2 < \omega^2 < \omega_T^2 + S/\epsilon(\infty) \equiv \omega_L \qquad (17)$$

Between ω_T and ω_L, the dielectric constant is negative. Wavelike solutions of the wave equation do not exist in this region, see Figure 9.

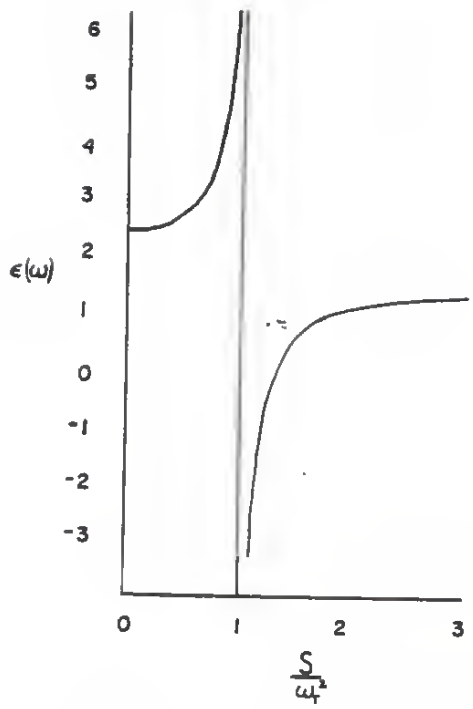

Figure 8. Dielectric constant in the vicinity of an absorption band. The plot of the dielectric constant was made by utilizing equation 16 with $S/\omega_T^2 = 1$ and $\epsilon(\infty) = 1.5$ [43].

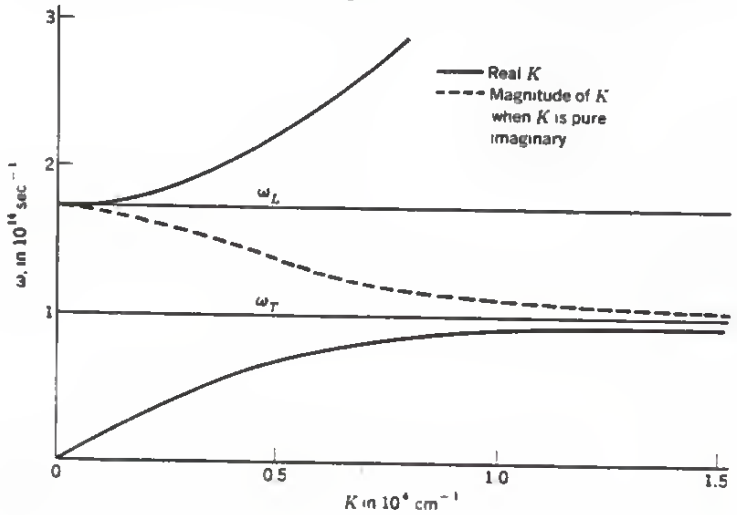

Figure 9. The forbidden zone. This is a plot of the frequency as a function of the dielectric constant. The broken line corresponds to absorption [43].

Furthermore, the refractive index is imaginary, $n = \sqrt{\epsilon}$. In this region, the reflectivity is high as evidenced by the imaginary refractive index. Therefore, in an infinite crystal, radiation of a characteristic lattice vibrational mode cannot be transmitted. Radiation will be both strongly absorbed and strongly reflected. This is the mechanism for restrahlen bands, German for residual rays. The reflection is coherent and therefore is regular reflection. In DRIFT, restrahlen bands are manifested as inverted peaks; ie., the reflection suddenly increases dramatically in what is otherwise an absorption peak.

As the thickness of the crystal is decreased, the assumption of an infinite crystal becomes no longer valid. Kittle cited experimental research as evidence that EM radiation of frequencies corresponding to the forbidden zone propagates through films which are approximately one wavelength thick [43].

3.3 *Freshnel Equations*

The mechanism for the rapid increase in the intensity of scattered radiation from the atom when $\omega \approx \omega_o$ has been discussed. The increase in the intensity of scattering is directly related to the increase in the intensity of the reflected radiation. Regular reflection from the surface is caused by coherent scattering from the oscillating electron clouds. This section is a quantitative analysis of the regular reflection from a surface. The incident EM field is divided into two perpendicular plane polarized electromagnetic fields, $E_{||}$ and $E_{\perp}$ (defined with respect to the plane containing the incident beam and the

reflectance beam). The reflectance from each is then calculated. The two reflectances are then added together giving the total reflectance from a nonabsorbing surface [18]:

$$R_{reg} = \frac{1}{2}\left[\frac{\sin^2(\alpha - \beta)}{\sin^2(\alpha + \beta)} + \frac{\tan^2(\alpha - \beta)}{\tan^2(\alpha + \beta)}\right] \qquad (18)$$

where α = angle of incidence and β = angle of refraction. Both α and β are measured form a line drawn perpendicular to the surface. For perpedicular incident radiation, $\alpha = 0$ and equation 18 simplifies to:

$$R_{reg} = \left[\frac{n_1 - n_o}{n_1 + n_o}\right]^2 \qquad (19)$$

Most non-absorbing materials have a index of refraction less than 2, so their regular reflection is also low. Using the mean value theorem and integrating equation 18 over the range 0 to $\pi/2$, Walsh calculated the regular reflection from a non-absorbing material [18] for diffuse incident radiation (see Table 2).

Table 2

Specular Reflectance From Nonabsorbing Surfaces

n	R_{reg} (perpendicular incident)	R_{reg} (diffuse incident)
1.00	0	0
1.50	.040	.100
1.60	.053	.107
1.70	.067	.121
1.80	.082	.134

The regular reflectance from diffuse incidence radiation is always greater than that from perpendicular incidence.

Earlier in the chapter it was shown that absorption bands affect the intensity of oscillations and make the index of refraction complex. The Freshnel equations may still be used, but "n" must be replaced by "n(1-iχ)", where χ is the absorption coefficient. The two components of reflection cannot be simply added, however, as they were in the nonabsorbing case. The complex refractive index affects each component of the incident EM field differently and they are not reflected in phase with one another. Second, the refractive index, n, is no longer constant but rather depends on the angle of incidence. Kortüm used two different methods to combine the equations [18]. The first does not provide any insight into the amount of reflected light and will be neglected in this paper. The second approach uses perpendicular incident radiation. At zero degrees incidence, the two components are

indistinguishable, since there is no longer any defined incident plane. The regular reflection is:

$$R_{reg} = \frac{(n_1 - n_0)^2 + (n_1 \cdot \chi_1)^2}{(n_1 + n_0)^2 + (n_1 \cdot \chi_1)^2} \qquad (20)$$

In the spectral regions where $n_1 \cdot \chi_1 >> n_1$, the reflectance is very high, approaching unity. Therefore, in the regions of strong absorption, the radiation is also strongly reflected.

The spacing of atoms in a crystal is very much smaller than the wavelength of IR radiation, about 5 orders of magnitude. Unless the incident EM field is perpendicular, the field will arrive at each successive atom at a slightly delayed phase. The subsequent emmanations from the atoms will constructively and destructively interfere. The constructive interference will produce a reflected ray and a refracted ray. From the theory of a classic harmonic oscillator, the intensity of displacement increases sharply when the frequency of the incident EM field is equal to a characteristic frequency; ie., an absorption band. Therefore, when an absorption band is encountered, the intensity of regular reflection increases dramatically and the intensity of the refracted or transmitted radiation decreases significantly. Furthormore, the transmission goes to zero when the frequency is in the forbidden frequency zone, unless the particles are small enough. If the particle size is on the same order of magnitude size as the wavelength

of radiation, the phenomena of reflection, refraction and diffraction are no longer seperately defined [18].

The oscillator model of a dielectric can also be used to provide a qualitative understanding of irradating a neat sample. When small particles are used, they will be in intimate contact with one another. While there will be many vacancies and pores, each gap will be very small as compared to the size of a particle. The particles will not oscillate as individual particles, but rather as a conglomerate of oscillators.

As the small particles are separated, the oscillators will only be influenced by other oscillators within the same particle. Since the particles are small, they will not radiate a completely coherent field. When the particle seperation is small, there will be interference of the radiation from adjacent particles, in much the same way as several antennas are used to produce a directional signal. There is still coherent scattering from the sample in this region.

As the particles are seperated still furthor, the coherent scattering effects will be eliminated. Therefore, it is essential that the sample particles be both small and isolated to avoid the coherent scattering effects for strong absorption bands. When these conitions are met quantitative theories of reflection are valid.

It should be emphasized here that the requirement for separation of the particles is only critical in regions where absorptions occur. Nonabsorbing matrix particles are in intimate contact with one another, but they are not intensely reradiating the incident EM radiation. This also means that a dielectric should be able to be used as the matrix as

long as the region of interest does not include the lattice stretching mode frequency. The lattice vibrations produce broad bands, but they are at a high frequency. For many of the surfaces of interest, the lattice vibrations will not interfere with the absorption bands being studied.

Chapter 4

Equipment

4.1 In-situ spectroscopy

In-situ spectroscopy involves heating the sample in a controlled environment. Numerous cells have been developed for that purpose [31,44,45,46,47,48,49,50]. The cells can be catagorized into two general groups based upon the method of heating the sample. The most common method is to move the sample into a furnace with a magnet or other device, heat the sample, and then move the sample into the beam of the spectrometer. The sample never leaves the controlled environment of the cell throughout the procedure. The other method is to encase the sample area and heat the sample while in the beam of the spectrometer. Hamadeh [12] singled out a cell recently developed by Hicks [47] as particularly promising for transmission IR studies of adsorbed species.

The principle difficulty in developing in-situ cells is caused by the poor thermal properties of the adhesives used to hold the windows on the cell [12]. The entire cell, including the furnace and cooling system, must fit in an sample area about five inches high for commercial spectrometers. DRIFT cells which are designed to fit in commercial spectrometers are constrained even more, because of the accompanying mirrors which must also fit in the sample area. DRIFT cells are capable of being heated in the spectrometer beam with the heater placed directly under the sample. Althouugh the conductivity is lower for a powder than for a pressed window, the distance over which heat is to be conducted is reduced by a factor of three or four.

At least four different in-situ DRIFT chambers have been developed [12,48,49,50]. Rein's cell made by Harrick Scientific Corp. is the in-sltu DRIFT chamber used ln this research [49]. An IBM praying mantis DRIFT accesory was modified to accomodate the cell.

4.2 Harrick high temperature vacuum chamber

The Harrick in-situ DRIFT chamber is designed to replace the sample area wlthln a praying mantis DRIFT accessory. In thls way, the Harrlck in-situ DRIFT chamber uses the optical configuration of the praying mantis accessory. Additional radlation is attenuated by constrlcting the beam to the two KBr windows, inlet and exit, of the chamber. Since the windows of the Harrick cell lie in different planes, the specular component is eliminated. There is concern that the SNR will be poor for this cell, particularly when a strong specular component is present [30]. The fraction of diffuse radiation from the sample area that will implnge on the KBr window, viewfactor, has been calculated by a Monte Carlo method (see appendix 2). The viewfactor of the exit KBr window was found to be 0.318 for radiation from the sample area. The radiation will be furthor attenuated at each of the KBr windows, about 4%. Therefore, even before considering any other losses it is only theoretically possible to collect 29% of the diffuse reflection, including diffuse Freshnel reflection. Although better SNR can be achieved through the optical configuration used by Hamadeh [30], sufficient radiation is expected wlth the Harrick ln-situ DRIFT chamber for acceptable SNR. A MCT detector and longer scan times are necessary to obtain a suitable SNR. An experimental approach is outlined in chapter 7 to

verify the amount of radiation lost by using the Harrick in-situ DRIFT chamber.

The sample area of the in-situ DRIFT chamber is positioned at the top of a post containing a resistance heater (see figure 10). A variable transformer has been used to provide the current for the heater. An iron-constantan thermocouple is built into the chamber and is attached at the base of the sample area. Extension wires are attached and which can be connected to an voltmeter to measure the E.M.F. Standard calibration tables are readily available for thermocouples. Actual measurements must be taken to determine the appropriate correction, ΔE [51]. Measurements have been taken by observing the micromelting point for various substances (see appendix 3). More complete experimental calibration can be accomplished using OMEGA temperature calibration laquers.

The top and the bottom sections of the cell are made of stainless steel. The top section is hollow and serves as a cooling jacket for the chamber, particularly the windows. A vitron O-ring seals the top and the bottom when assembled. The KBr and glass windows can be sealed with silicon grease. If the sample is heated above 300 C, however, the vitron O-rings need to be used [49]. Kalrez O-rings will extend the maximum temperature higher yet. Copper gaskets can be used for spectra taken under ultra-high vacuum.

Emission from the sample and from the top of the post can be a problem at elevated temperatures. Since the sample area is between the interferometer and the detector, the emission will be unmodulated. It

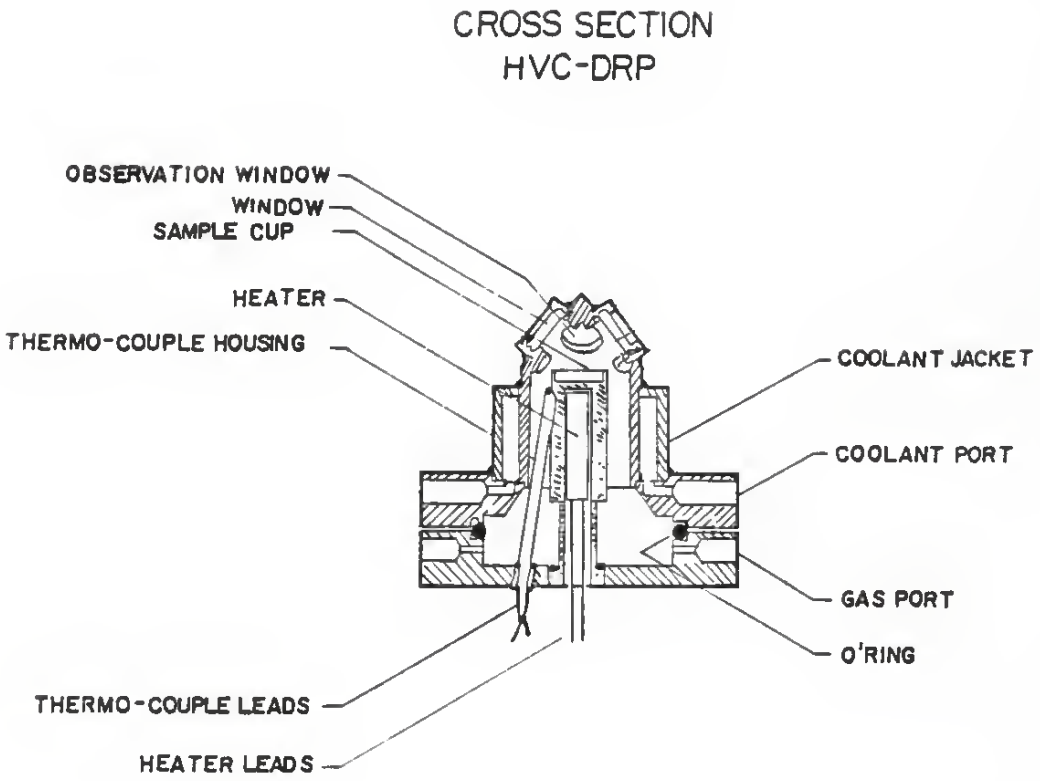

Figure 10 Harrick in-situ DRIFT chamber. This figure is a cross section of the HVC-DRP in-situ DRIFT chamber marketed by Harrick Scientific Corp [49].

will not be included as part of the interferogram, but can cause excessive heating of the detector. Hamadeh installed a mica washer around the top of his sample cup to reduce the emission of radiation [30].

4.3 Modifications to Equipment

The in-situ DRIFT chamber replaced the regular sample cup of the praying mantis DRIFT accessory. The back of the praying mantis accessory was cut out to accomodate the cell (see figure 11). Next, a method was needed to suspend the chamber in the proper position. An analysis of the required sample position, the size of the chamber and the position of the ellipsoidal mirrors showed that the chamber would have to be lowered while moving it to and from its sampling position.

The cradle is moveable in all three directions to position it for the maximum signal (see figure 12). The cradle rests on a plate which is attached to a x-y traversing mechanism. This mechanism is attached to an aluminum bar. The aluminum bar moves in the z direction. Oversized brass nuts (round, about 1" in diameter) suspend as well as move the aluminum bar.

It is essential that the sampling location be fixed for each spectra. Once the sample cup is positioned in the x and y directions, these knobs are no longer used. The cradle need only be raised and lowered to change the sample. A pair of locking nuts limit the upper position of the bar, marking the sampling location. When the cradle is down, the cell can be removed or replaced without disturbing the cradle.

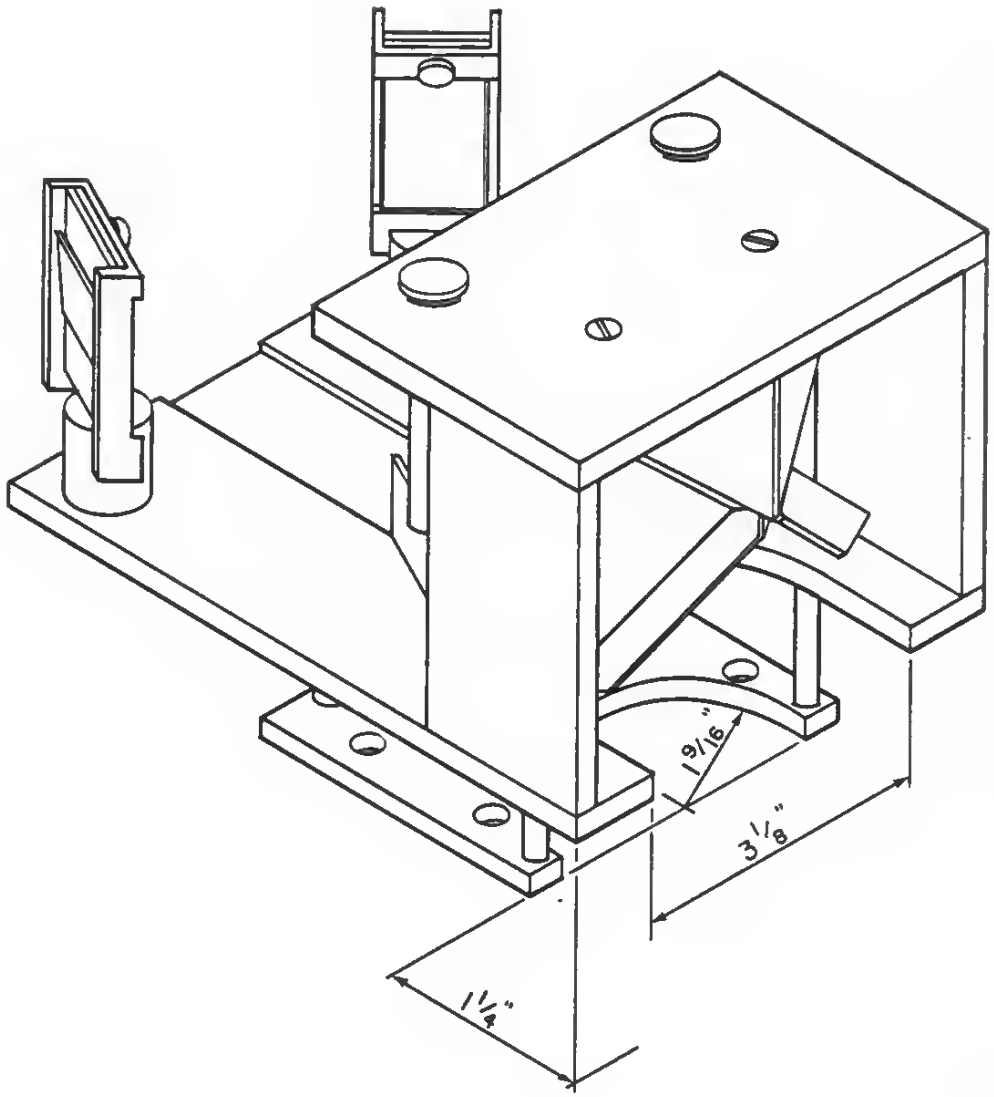

Figure 11. Modified IBM praying mantis DRIFT accessory. The sample cup of the in-situ DRIFT chamber fits into the same place as the sample cup which has been removed fitted. A section was cut out to make room for the in-situ DRIFT chamber.

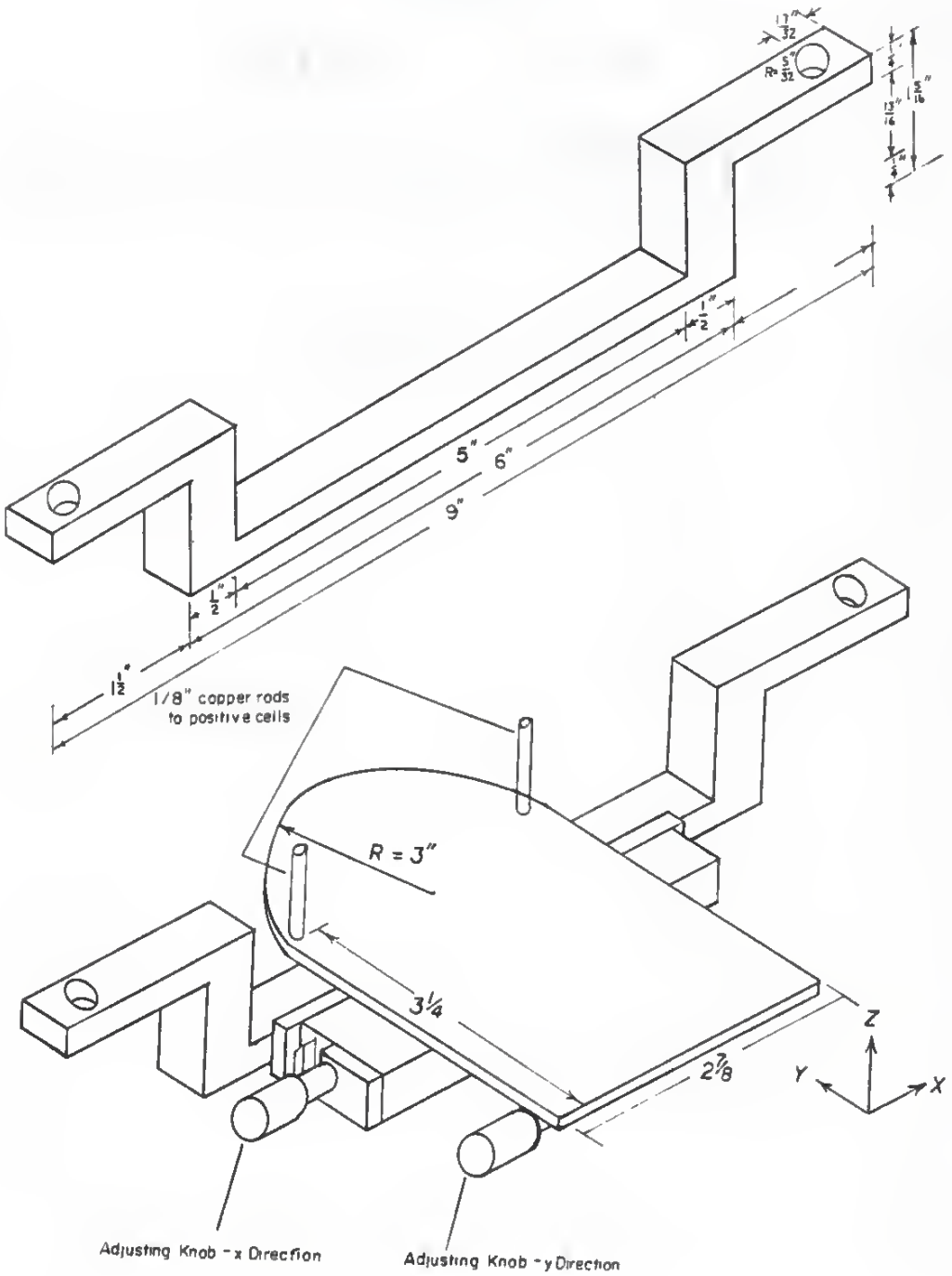

Figure 12. Cradle for in situ DRIFT chamber. This apparatus is designed to hold the in-situ DRIFT chamber, (see figure 10), at the proper location with respect to the DRIFT accessory.

Two small vertical brass rods mark the position of the cell on the cradle. Once the DRIFT accessory and the in-situ chamber are properly aligned with the spectrometer, a small external piece must be attached to the in-situ chamber lower section. The purpose of this piece is to provide an exact reference for the placement of the chamber on the cradle. The cell can then be placed on the cradle plate and turned so theat this added piece rests against one of the two small brass rods.

A new aluminum base plate was cut out for use with tbe aluminum bar and cradle. The base plate sets the position of the praying mantis accessory within the spectrometer sample area. Two vertical bolts were attached to the base plate to guide the aluminum bar (see figure 13).

The IBM FT-IR spectrometer operates under a vacuum. Therefore, the electrical wires and tubing used for the in-situ chamber would have to be introduced through the aluminum plate at the side of the sampling compartment. Bulkhead adapters were placed in holes through the aluminum plate to provide access while maintaining the vacuum (see figure 14). The gas lines are 1/8 inch copper tubing. Tygon tubing is used for the water cooling lines, because of the requisite flexibility needed. Imperial brass bulkhead adapters with plastic "clamps" are used to insure a good seal. A leak cannot be tolerated. The thermocouple and heating element wires were sealed with epoxy on each end with Superglue completely filling the center. The tubes and wires are passed through the aluminum plate without breaching the vacuum.

Pictures of the completed modifications are provided at the end of this chapter (see figure 15, 16).

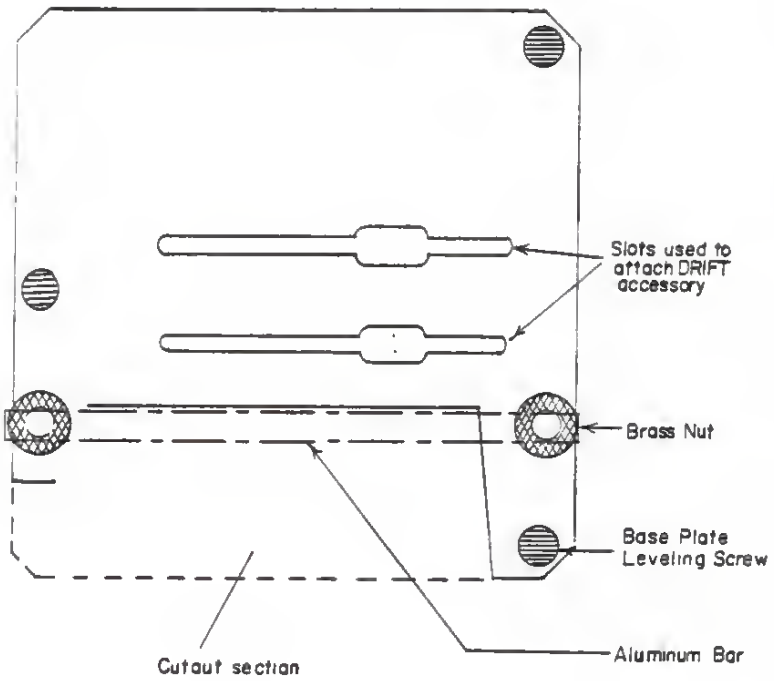

Figure 13. Modified base plate. A new base plate was designed for use with the cradle shown in (see figure 12). The DRIFT accessory rests on the baseplate.

Figure 14. Aluminum plate with bulkhead adapters. This modification allows access to the in-situ DRIFT chamber without interupting the vacuum of the interferometer.

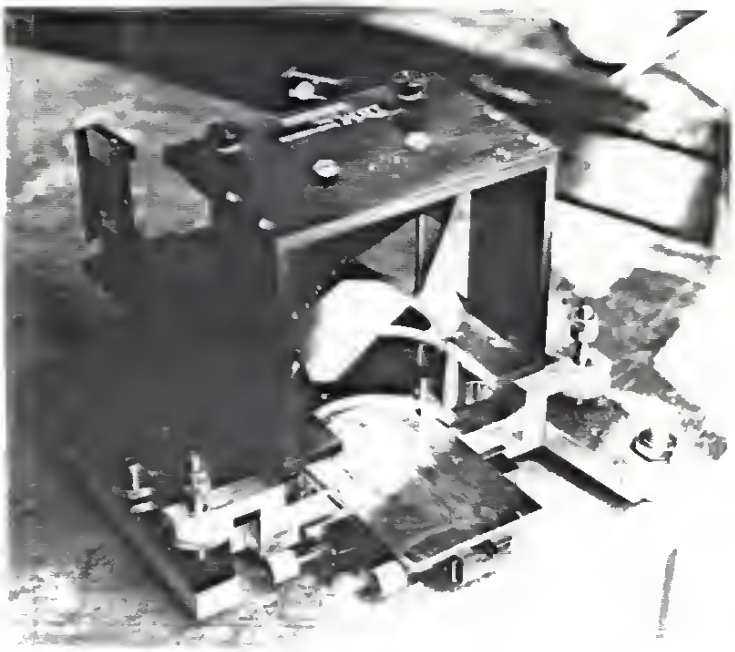

Figure 15. Picture of the modified praying mantis DRIFT accessory.

Figure 16. Picture of the modified praying mantis DRIFT accessory with the in-situ chamber in place.

Chapter 5

Alumina

5.1 Choice of initial catalyst system for study

Once the Harrick in-situ DRIFT had been installed, a suitable test of the installation and capabilities of the cell was needed. Extensive research had just been completed by Larry Sampson and John Matthews on the disproportionation of CO on alumina. Sampson studied the structure and preparation of several alumina phases. He demonstrated that an amalgamated preparation procedure could be used to produce well characterized aluminas (bayerite, boehmite, η-alumina and γ-alumina) [52]. The transition from bayerite and boehmite to η- and γ-alumina, respectively, takes place at 550° to 600°C [52,53]. The transition involves the dehydroxylation of the lower temperature phases to form the transition aluminas. Each of these phases have been studied independantly, but no previous IR studies have been made of the transition from one phase to another. During dehydroxylation, stuctural oxygens are lost resulting in a change on the crystal structure, a transition to the new phase.

The transition takes place within the stated temperature capabilty of the cell (more than 600°C [49]). The exit port and gas line will be attached to a pump to evacuate the desorbed water. No other special equipment or materials are needed such as a fume hood or reactants. In short, simple dehydroxylation appears to be an excellent test for the capabilities of the cell. Finally, the IR study of this transition

should shed further light on the nature of the hydroxyl groups in the transition aluminas.

5.2 Alumina

This section will provide an introductory look at aluminas. Additional information is available in many sources (52,53,54,55). Alumina is a generic term for aluminum oxides and hydroxides. The stoichiometric fnrmula for these materials is $Al_2O_3 \cdot n(H_2O)$, where n=0 to 3. There are at least five thermodynamically stable transition phases and several more transition phases (see figure 17). Boehmite gel, listed in figure 18, is also called pseudoboehmite. Throughout this paper the term, boehmite, will only refer to crystalline boehmite. The properties of the low temperature phases and α-alumina have been reviewed in depth by ALCOA [51]. The surface properties of the transition aluminas bas been reviewed by Knozinger [56]. Except for α-alumina, corundum, each phase possesses surface hydroxyls. In general, the aluminas strongly adsorb water. The structures of bayerite and boehmite are not completely understood, because their crystal size is too small for structural analysis (less than 10 microns in diameter) [52]. The structures of bayerite and boehmite have been estimated through comparison with nther phases, gibbsite and lepidncrocite, respectively. Both η-alumina and γ-alumina possess a defect spinel structure. η-alumina has a strong one dimensional disorder of the cubic-closed-spaced lattice [52].

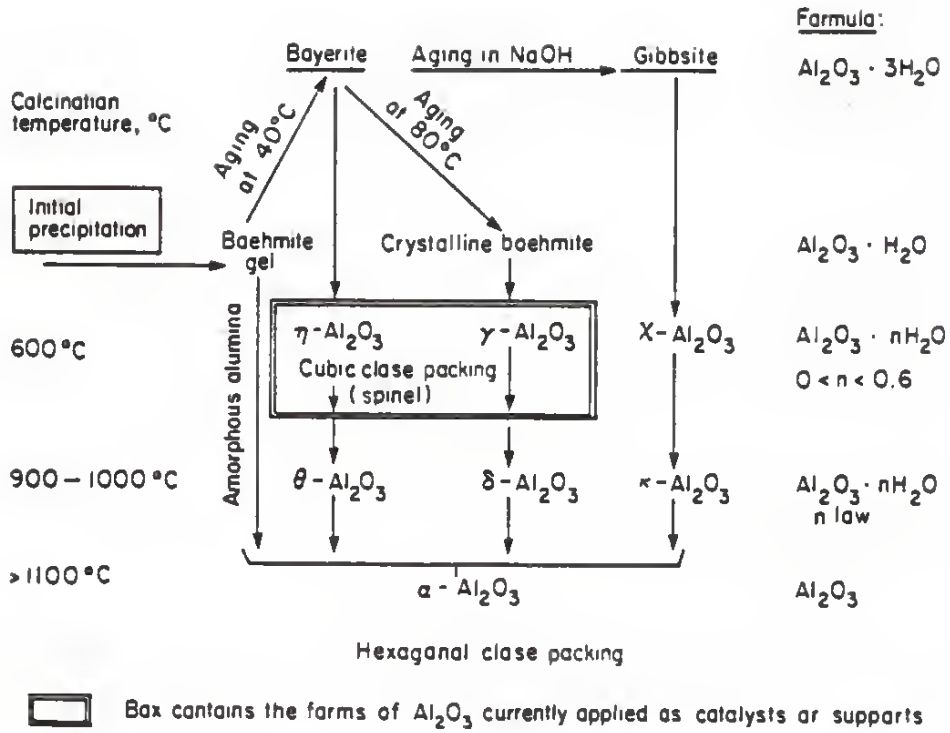

Figure 17. Schematic of the Alumina phases. This diagram illustrates the interrelationship that exists between the various alumina phases. The degree of hydroxylation of each is indicated at right [53].

Extensive research has been done trying to determine the nature of the surface of alumina and other oxides. η- and γ-alumina have received the principle focus, because of their role as catalysts and catalyst supports. A strong case has been made that the (111-) and (110-) faces form the surface layers of η- and γ- alumina, respectively [56].

5.3 Preparation procedure

An analgamated process was used to make the alumina [52]. First, one-to-two inch square sheets of 99.99% pure alumina foil from Allied Chemical were lowered into a beaker containing dilute hydrochloric acid (1 part concentrated HCl mixed with 3 parts water) floating on Mercury. This was done to remove the oxides from the surface of the alumina before lowering it into the Hg. While holding the alumilna squares down with glass rods, the HCl was decanted off and then replaced with distilled water. Then the foil squares were taken from the Hg and placed in a beaker containing distilled water, either at room temperature or at 90°C. The squares that were placed in water at room temperature began to react slowly releasing gas bubbles. As the water heated to 57°C the reaction became much more rapid. This reaction turned the water to a dark grey. By the second day, all of the samples had become light grey and was suspended in the water. The water contining suspended alumina was removed, leaving bulk mercury which was washed and returned to the beaker containing Hg. The solution was dried at 30°-40° for two weeks leaving a white precipitate. Analysis by x-ray diffraction confirmed that the sample was bayerite (a trihydroxide crystalline alumina).

Other amalgamated alumina squares were placed in distilled water at 90°C. The reactlon began to take place lmmediately, releasing suffi-clent gas to give the appearance of bolllng. The bulk of the reaction took place ln 30 minutes. The water became light grey in color and remalned that way throughtout the reaction. Again the suspenslon was separated from the Hg and any unreacted resldue by decanting. The suspension was contlnuously heated at about 90°C until dry. The precipitate was a very falnt rose color. X-ray analysis confirmed that this sample was boehmite (a crystalline alumina oxlde hydroxide).

The bayerlte and boehmite were further calcined in a muffle furnace at 550-600°C overnight. The resulting materlals were η- and γ-alumina, respectlvely. These transitlons were also confirmed using x-ray dlffraction. Each of the 4 samples were stored ln a dessicator contain-ing Drierite to reduce the adsorptlon of water during storage.

Chapter 6

Alumina Spectra

6.1 Mid-IR region

The middle of the IR region (2.5 to 15 μm) is by far the most commonly used region in IR spectroscopy. Fundamental vibrational transitions occur in both the mid- and far- (12.5 to 300 μm) IR regions, but the far-IR region is much less accessible. Inorganic compounds have less energetic vibration modes than organic compounds and are therefore at longer wavelengths, extending into the far-IR. For dielectrics, the stretching vibration modes also mark the end of their transparent region. For example, the alumina lattice stretching modes occur around 13 μm, which also corresponds to the frequency region where aluminas are no longer transparent. These lattice vibrations absorb strongly, exhibiting the resonant effects discussed in Chapter 3. The strong reflection that accompanies these absorption bands makes it exceedingly difficult to study the effects of a particular pertubation on the Al-O stretching absorption band. Each spectrum has been placed at the end of this chapter (figures 18 to 33).

6.2 Mid-IR transmission spectra of alumina

6.2-1 Previous mid-IR research with aluminas

Most mid-IR spectra have been obtained through transmission spectroscopy. Numerous transmission spectra are available to characterize many of the absorption peaks for different aluminas (see table 3).

Table 3

Reference Absorption Peaks (mid-IR)

(wavelength μm)

Phase	OH stretch	O-H bend	Unassigned	Al-O stretch	Reference
Bayerite	2.74, 2.830 2.842, 2.895 2.94	9.84	11.16, 12.3	12.88	[53,61,62]
Boehmite	3.02, 3.247	6.75, 9.35		13.5	[53,61,62]
η-Alumina	2.642, 2.674 2.695				[61a]
γ-Alumina	2.635, 2.646 2.678, 2.679 2.704				[25]
α-Alumina			15.58, 16.61 17.89, 20.41 22.21	13.16	[62,62a]

Mid-IR spectra reveal differences in the hydroxyl groups and the Al-O groups within the various alumina. The degree of dehydroxylation is also manifested in changes of the hydroxyl stretching region (2.6 to 3.6 μm). Water is desorbed into the gaseous phase as the sample is heated, particularly when the heating is done under vacuum. Transmission spectra for the transition aluminas have been recorded after evacuation at elevated temperatures ranging from 100° to 900°C [25].

The hydroxly group stretching mode absorptions have received the principle interest during IR studies of alumina. Frederickson used the O-H stretching and bending adsorption bands to distinguish various bauxite ores [61]. Low temperature aluminas such as bayerite, boehmite and various natural occurring aluminas possess several different O-H stretching mode absorption peaks under atmospheric conditions. Assignments of these absorptions to a particular surface geometry have not been found. Transition aluminas, on the other hand, do not exhibit any isolated hydroxyl groups until they are dehydroxylated at elevated temperatures [25].

The transition aluminas and other oxides have been studied extensively to ascertain the nature of catalytically active sites. These aluminas are activated through dehydroxylation. At least three chemically distinct isolated hydroxyl peaks remain after the alumina has been dried at 650°C [25]. Five absorption peaks can be observed for very dry samples between 3690 and 3600 cm^{-1} [25]. The last two peaks are weak and are typically difficult to resolve because of the overlap with stronger peaks.

These observed peaks have been related to proposed surface structures. In general, the surface structures are modeled as an extension of the bulk structure. Peri assumed that the (100)-face was exposed and simulated dehydroxylation using a Monte Carlo simulation [64]. From the pseudomorphosis considerations of Lippens [62], catalytic and surface chemists [62a] have concluded that the exposed face for η- alumina might be the (111)-face. They have also concluded that either the (110)- or the (100)- face might be the exposed surface layer for γ-alumina. However, the surface structure of alumina may be more complex and may not be adequately modeled by an extrapolation of the bulk structure.

Knözinger and Ratnasamy reviewed research on the hydroxyl groups of alumina [62a]. Their analysis centered around the net charge on an O-H group and assigned each possible configuration for the (100)-, (110)- and (111)- exposed crystal faces. The procedure involved analyzing the number of Al^{3+} cations coordinated with each oxygen, as well as the structural configuration; ie. octahedral or tetrahedral. When the net charge on O^{2-} is more negative, the absorption will be shifted to higher wavenumbers. They correlated each possible OH configuration with a particular absorption peak (five different absorption bands). They deduced that defect sites are created during the dehydroxylation and that these defect sites account for the catalytic activity. However, the very existance of charge defects is not certain [24]. Furthermore, no quantitative relationship has been shown between the proposed charge defect and the vibrational band shifts observed with infrared

spectroscopy. In addition to charge defects, hydrogen bonding to other hydroxyl groups and other factors can appreciably shift absorption frequencies. In short, Peri states that the assignment of hydroxyl groups must be tentative at present [24].

Various probe molecules have been utilized to analyze alumina. CO_2 has been one of these probe molecules. It is readily absorbed by alumina, even from the atmosphere. Knözinger reviewed research on the poisoning of oxide surfaces by adsorbed species [63]. Adsorbed CO_2 possesses an asymetric stretching mode which corresponds to a sharp absorption band that has been observed at 4.47 μm [66] and 4.22μm [68]. CO_2 absorption onto oxide surfaces can lead to a variety of possible carbonate species [63]. Each carbonate species posseses absorption bands between 1900 and 650 cm^{-1}. For example, unidentate carbonate has six vibrational modes which absorb between 1530 and 670 cm^{-1}[63]. The structure of the solid phase does not influence the spectra significantly. Each of the five transition aluminas (γ-, δ-, θ-, κ- and χ- alumina) that had been studied behaved in much the same way [63].

The Al-O stretching mode vibrations also correspond to absorption within the mid-IR region of the spectrum. Each phase absorbs at different wavelengths. One stretching absorption peak has been identified between 13 and 14 μm for each of the aluminas in ALCOA technical paper number 19 [54].

In addition to the above known absorption peaks, several unidentified peaks are present [54]. Many of these peaks are in the region

between the absorption peaks corresponding to hydroxyl bending and the absorption peaks corresponding to Al-O stretching. Others are at wavelengths shorter than the peak associated with AL-O stretching.

6.2-2 Observed transmission spectra for alumina samples

Each of the aluminas phases prepared in this research was confirmed by x-ray diffraction. Transmission IR spectra were obtained for the well characterized alumina phases prepared by the amalgamated procedure as references for future work (figures 20 to 24).

Two spectra were taken for each of the four aluminas with a Perkin Elmer 180 spectrometer (see table 4). The samples were prepared as a KBr/sample pressed disk and as a NUJOL mull. Each of the samples except for bayerite was dried at 100°C. They were then placed in a desiccator under vacuum. While preparing the mulls and pressed disks, both the sample and the KBr were exposed to the air. Each spectra was obtained at room temperature. The spectrometer was purged with dry air while obtaining the spectra.

6.2-3 Interpretation of mid-IR spectra

Many common features are present in each of the observed transmission spectra. A broad band centered around 2.9 to 3.0 μm corresponds to hydrogen bonded hydroxyl groups. The O-H absorption peak for adsorbed water will also absorb in this same broad region. The Al-O stretching mode vibrations occur at 13 to 14 μm. Only one absorption peak for each phase was identified as Al-O stretching in the ALCOA technical paper. Since there are more than one different Al-O configurations in the

Table 4

Observed Transmission Absorption Peaks (mid-IR)
(wavelength μm)

Phase	OH stretch	O-H bend	Unassigned	Al-O stretch
Bayerite (fig. 20)	2.74#, 2.630## 2.93##, 2.940*, 2.92	9.6, 9.9## 10.4##	6.13, 19.4 24.7	13.25, 14.2
Boehmite (fig. 21)	2.74, 2.82, 2.69 3.04*, 3.23*	6.7*, 9.45* 10.15*	16.15, 21.2	14.0
η Alumina (fig. 22)	2.9 (broad)		4.77, 17.5 6.22, 7.3	14.0
γ Alumina (fig. 23)	3.02 (broad)	9.45 ?	16.7	13.60
α Alumina	2.97 (broad)		16.7	13.2*

* Correspond to peaks in paper by Frederick [61]
\# Correspond to peaks from Sadtler reference spectra [62]

Instrumental information for transmission spectra

Beekman 180 Grating Spectrometer		Constant I_o mode	
Resolution	2.6 cm^{-1} @4000 cm^{-1}	Slit width .2 mm @ 4000 cm^{-1}	
Scan Time:		Slit program	5
Fine	5.0	Suppression	10.0
Coarse	10.	Parameter mode	A
Time Constant	5		

structure of alumina, other peaks are expected. Numerous unassigned peaks are given for each spectra, particularly at longer wavelengths, 15 to 25 μm. Some of these unassigned peaks probably correspond to Al-O stretching modes.

The obseverved absorption peaks for bayerite and boehmite correspond to those previously cited in the literature. In boehmite, there are four additional sharp peaks with shorter wavelengths than those cited. The peak observed at 2.74 μm corresponds to a wavelength at which isolated hydroxyl groups absorb radiation. The observed Al-O stretching mode absorptions are at slightly longer wavelengths than those cited in the ALCOA technical paper [54].

The spectra from the transition aluminas are difficult to analyze. The hydroxyl stretching peaks cited in the literature correspond to samples which have been dehydroxylated. As expected none of the isolated hydroxyl absorption peaks can be observed in these samples since they were only heated to 100°C. None of the references cited Al-O stretching absorption peaks. The absorption peaks at 14 μm for η- and at 13.80 μm for γ-alumina correspond to Al-O stretching absorption peaks in the other aluminas. The weak absorption peak at 4.77 μm for η-alumina probably is due to adsorbed CO_2.

6.3 Mid-IR ORIFT Spectra of Alumina

DRIFT spectroscopy is a relatively new analytical tool. Few references have been found in the literature. One reference is available in which ORIFT spectroscopy is used to study an alumina. An

amorphous alumina gel with varied properties was used. The properties of the gel were a function of pH during the sample synthesis [67].

6.3-1 Observed mid-IR DRIFT spectra for alumina samples

Some DRIFT spectra were obtained before the spectrometer cooling line burst; boehmite (neat), gamma (2.6% in KBr) and gamma (neat) (see Table 5 and figures 23 to 25)). The IBM-98 FT-IR spectrometer was evacuated for 15 to 20 minutes before irradiating each sample. Each sample had been open to the air while being prepared in the sample cup.

6.3-2 Analysis of mid-IR DRIFT

The hydroxyl stretching frequencies are generally the same as thnse in the transmission spectra. The relative intensity of the peaks differs, but this is expected. The two main hydroxyl stretching peaks of boehmite are observed in the DRIFT spectra at the same frequency as the transmission spectra. The smaller peaks of higher frequency that had been observed with transmission spectroscopy are present, but very weak.

The SNR is proportional to the sample concentration for transmission spectroscopy in the limit of low sample concentration From the Beers-Lambert law:

$$-\log_{10} T = a \cdot b \cdot c \qquad (21)$$

where T is the transmittance, a is the absorptivity and b is the path length Therefore:

Table 5

DRIFT Absorptioo Peaks (mid-IR)
(wavelength μm)

Phase	OH stretch	CO_2 stretch #1	unknown #2	OH bend #3	unknown
Boehmite (Neat-100%)	2.72, 2.74	4.76	6.08	9.0(s)	10.6(s)
(neat-100%)	2.76, 3.02(s)		6.69	10.1	
(figure 23)	3.23(s)				
γ Alumina	2.64, 2.65	4.26	6.85	6.51	11.72 #4
(2.76%)	2.71, 2.77		7.34		
(figure 24)	2.64(broad),2.95				
γ Alumina (neat-100%)	2.71	4.26	7.2	6.5	9.5(vs) #5
(figure 25)	2.64(broad)		7.4		

#1- asymetric CO_2 stretching mode of an undissociated CO_2 molecule adsorbed on the surface [66,86]

#2 - May be due to CO_2 adsorbed and held as carbonate ion, unidentate carbonate, bidentate carbonate or bicarbonate [66]
Another possibility is the first overtone of the Al-O lattice stretching mode.

#3 - probably OH bending mode based on references $\delta_{O-H} \rightarrow 8.7\text{-}10.15\ \mu m$

#4 - Probably a lattice absorption peak at 11.72 μm. This is a shorter wavelength than specifically identified for Al-O stretching in the literature. It is too strong to be associated with the hydroxyl groups.

#5 - An anomalous peak associated with the restrahlen effect.

Instrumental Information for mid-IR DRIFT

IBM 98 FT-IR w/Giozel type interferometer
Glober source - IR Associates & Co., IMC
High frequency cutoff- 4500 cm^{-1}
Optical velocity - 1.582 cm/s
scans per spectra- 100
Equipment Operator - Daimay L. Vein

K8r Beamsplitter
Resolution - 4 cm^{-1}
Aperture - 1.2 μm
Appodization function - boxcar
Zero filtering factor - 2

$$T = 10^{-abc} = e^{-2.303 \cdot abc} \tag{22}$$

$$= 1 - 2.303abc + 2.651\ a^2b^2c^2 \tag{23}$$

The absorptance, 1-T, is given in the limit as c tends to zero as 2.303abc, so that the SNR is linearly proportional to the concentration. For transmitance, Whereas, the SNR (the measured signal is the reflectance for DRIFT) is proportional to the square root of the sample concentration for DRIFT spectroscopy (Kubelka-Munk Theory). Therefore, DRIFT is more sensitive to impurities or surface anomalies than transmission spectroscopy. There is a shoulder at 2.68 μm (3730 cm^{-1}) in the DRIFT spectra of the neat γ-alumina. This corresponds to one of the three strong isolated hydroxyl peaks observed in dehydroxylated γ-alumina by Peri [26].

Several absorption peaks are observed in the DRIFT spectra that are not visible in the transmission spectra. The absorption peaks at 4.26 μm in γ-alumina and at 4.78 μm in boehmite corresponds to the asymetric stretching mode for adsorbed CO_2. The absorption peaks between 6 and 7.4 μm could be one of the adsorbed carbonate forms that often accompanies the adsorption of carbon dioxidete. The first overtone of the Al-O stretching mode should also occur in this range (½ of the fundamental wavelength). This observation has not been confirmed through any published sources. However, the strength of the fundamental absorption band makes this a possibility.

The low energy modes, below 8.5 μm (1175 cm^{-1}), are a problem area. The Al-O stretching vibration absorbs radiation of its characteristic frequency very strongly. Subsequently, the resonant effects outlined in Chapter 3 are present in its spectra. This is most clearly illustrated with the γ-alumina spectra (see figure 26). In the range 1800 to 800 cm^{-1}, the transmittance of γ-alumina drops to zero followed by a sharp increase in transmittance at 1000 cm^{-1} or 10 μm. This is the outward manifestation of a restrahlen bond [69]. The expanded spectra of 2.76% γ-alumima provides additional insight (see figure 27). There are absorption peaks in this region with a strong absorption peak beginning at 1000 cm^{-1}. There is a strong peak at 833 cm^{-1} on the edge of what appears to be a still stronger absorption peak. In the neat DRIFT spectra these peaks appear to be less intense than the very strong peak at 9.45 μm (1050 cm^{-1}). The smaller peaks at 10.8 and 11.7 μm (930 and 850 cm^{-1}) are probably linked to the actual absorption peaks, but additional spectra are necessary for verification. The 9.45 μm peak for the neat γ-alumina is an anomalous peak, not corresponding to any absorption peak in the more representative dilute spectrum. The absorption wavelength must be taken from the 2.76% concentration spectra to insure the right peak is selected.

Based on the strength of the absorption band, the peak at 11.7 μm (see figure 27) probably corrresponds to a vibrational mode. This peak is on the shoulder of a still greater peak, which corresponds to the wavelength observed in the transmission spectra. Neither hydroxyl

bending modes nor adsorbed species possess that large of an absorption intensity.

6.4 Near-IR Region

The near-IR region (0.7-3.0 μm) of the spectrum has been used extensively to analyze fat, protein and moisture in foodstuffs [70,71]. Strome and Klier used the near-IR region while investigating photoluminescence and resonance energy transfer in a NaY zeolite [72]. Otherwise, this region has received little emphasis in the study of catalysts and adsorbed species. The near-IR region of the spectrum corresponds to overtones and combinations of vibrational transitions. Given a characteristic vibration, bigher order vibrations at 2,3,4... times the characteristic vibrational frequency occur and are called over-tones. Combination frequencies are the result of the linear combination of the stretching and bending mode vibrations of a particular group of atoms. There is a rapid decrease in intensity as the nrder of the overtone is increased. Only the first and second overtones can normally visible. The functional groups that can be observed in the near IR are limited to X-H groups (where X = C,O,N,S, etc.) and carbonyls. [73]

The near infrared region offers better optical properties than the mid-IR region, which in turn results in more signal and a better SNR. The detectors used in the near-IR region are more sensitive than the thermal, photoconductive, or photovoltaic detectors used in the mid-IR region. The transmissivity of the optical components is higher at the shorter wavelengths of the near-IR region. This includes the beam

splitter, the numerous mirrors and the windows that interrupt the incident and reflected beams. Near-IR instruments can achieve about 10 times better resolution than good laboratory mid-IR instruments [73]. This improved resolution has not been fully utilized in studying adsorbed species and may prove to be a powerful tool.

There is far less information available concerning near-IR spectra. Pasto's organic spectroscopy book tabulates near-IR absorption bands on a bar chart [73]. Some research has been performed with silicates and zeolites in which the near-IR region was used. The stretching vibration overtone band, 2ν , for water occurs at about 1.4 μm [74,75]. This is expected to be a broad band in accordance with the fundamental absorption band observed wavelength in the mid-IR region. The 2ν absorption band for isolated hydroxyl groups is located about 1.37μm [74]. The combination band, $\nu + \delta$, is expected around 1.9 μm. [75]. Since each of the near-IR spectra correspond to spectra taken in the mid-IR region, the overtone absorption band locations can be closely approximated by calculating a predicted value from the observed mid-IR peaks.

6.4-1 Observed near-IR DRIFT spectra of alumina

While conducting this research, a near-IR DRIFT spectrometer was made available by the U.S. Grain Marketing Research Labaratory in Manhattan Kansas. Four different samples were scanned with a Technicon 500 near-IR diffuse reflectance spectrometer (bayerite, boeh-mite, γ-alumina and commercial γ-alumina) to develop a broader understanding of the usefulness of near-IR spectroscopy in analyzing oxides. Additionally, bayerite and boehmite were scanned with the DIGILAB 155

FT-IR, equipped with a Barnes DRIFT collector. The bayerite, boehmite and γ-alumina were prepared according to the amalgamated procedure outlined in Chapter 5. The samples were ground and then sieved with a number 240 sieve (less than 53 μm in diameter). The α-alumina was produced by Alfa products with particles smaller than 10 μm in diameter.

The two spectrometers are significantly different. The Technicon near-IR DRIFT spectrometer has been designed to analyze many samples rapidly, as in a commercial laboratory. The software is user friendly, requiring the operator only to specify the resnlution and the spectral region of interest. This also limits the flexibility in adjusting the equipment. The software provides far less capability to manipulate the interferogram. Two spectra were taken from each of the four samoles scanned with the Technicon spectrometer. Before the second spectra was taken, the sample was rotated 90°, to check the sample packing for specular effects. No change was observed for any of the samples. The absorption peaks have been tabulated (see Table 6).

The DIGILAB spectrometer is significantly more complex to operate, but provides greater capabilities. The optical configuration is better, providing more radiation and therefore a better signal-to-noise ratio. The DIGILAB spectrometer can be adusted to provide better resolution than the Technicon spectrometer. In addition, the software is much more flexible. Subsequently, the spectral features can be deconvoluted by manipulating the interferogram. Various apodization functions can be used to minimize the effects of finite scan times. An appodization function is a particular function that is multiplied with the interferogram. It is used to reduce the effects of ringing and peak

broadening created because the interferogram was obtained in a finite amount of time. The SNR is also improved through the use of an apodization function.

Only bayerite and boehmite were analyzed with the DIGILAB spectrometer. The overtone absorption peaks can be readily correlated from their fundamental absorption peaks. There can be a small frequency shift from that predicted by taking one half of the fundamental wavelength. When there are multiple hydroxyl peaks, combination peaks probably will not be able to be identified with their specific fundamental peaks. Although complete spectra were obtained, only the region from 1.351 to 1.538 μm was plotted (see Table 7).

6.4-2 Analysis of near IR alumina absorption peaks.

The strongest absorption peak for any of the spectra is at 1.39 μm in boehmite. There is not a strong absorption, however, near 2.78 μm in the mid-IR. There is either a significant frequency shift, i.e. possible from 3.02 μm or there is an enormous deviation from intensities for these overtone peaks. The frequency shift is probably the most accurate description. In bayerite the strongest three overtone bonds have been shifted by 10 to 20 μm to a shorter wavelength from ½ ν. The mechanism for frequency shifting is not understood nor is the mechanism for the intensity expected understood. Overtone absorption bonds are broader and separated better than their corresponding fundamental absorption bands. Some of the shoulders in the mid-IR correspond to an absorption peaks in the near-IR region. Overall, the correlation

Table 8

Near-IR ORIFT abaorption peaks (Technicon 500)
(wavelength μm)

Phase	2ν	Combination band ($\upsilon+\delta$)	Other Combination bands
Bayerite (figure 24)	1.400,1.434 1.448,1.514	1.940	2.214,2.280 2.388,2.424
Boehmite (figure 25)	1.394,1.435 1.450,1.589		2.208,2.256
γ-alumina (figure 26)	1.384	1.884	2.244
α-alumina (figure 27)	1.410	1.944	

Technicon 500 Near-Infrared Analyzers
1100-2500 nm 4-nm resolution
references:
A= 1.0 carbon black
A= 0.0 teflon

Table 7

Near-IR ORIFT absorption peaks (OIGILAB 15S)
(wavelength μm)

	Strong	Medium	Shoulder	Other
Bayerite (figure	1.414, 1.43 1.453	1.385, 1.513	1.387, 1.379 1.396	1.371,1.414
Boehmite	1.393	1.435, 1.453	1.381, 1.379 1.43	1.37, 1.382 1.415, 1.513

Instrumental information for near-IR DRIFT spectra with DIGILAB spectrometer
Digilab 15S FT-IR Barnes analytical collector ORIFT accessory
resolution 4 cm^{-1} 10,000 to 4000 cm^{-1} (only 2υ, plotted)
Source 50 W halogen lamp Quartz beamaplitter
PbSe detector
deconvolution-DIGILAB software [73a]

between observed overtone absorptions and the predicted overtone location is good.

The increased separation of peaks in the near-IR region provides invaluble insight into the O-H stretching region. This is more clearly visible with the spectra obtained and deconvoluted with the DIGILAB spectrometer. There is a significant difficulty in relating a particular near-IR peak with its corresponding fundamental absorption peak. Furthor insight into the frequency shifts that occur for the overtone bands is needed. Research is also needed to predict which fundamental peaks possess overtones which will be visible. In many cases, the same spectrometer can be utilized for both spectra. The spectrometers are changed from one spectral region to another by changing the source, the detector and the beamsplitter.

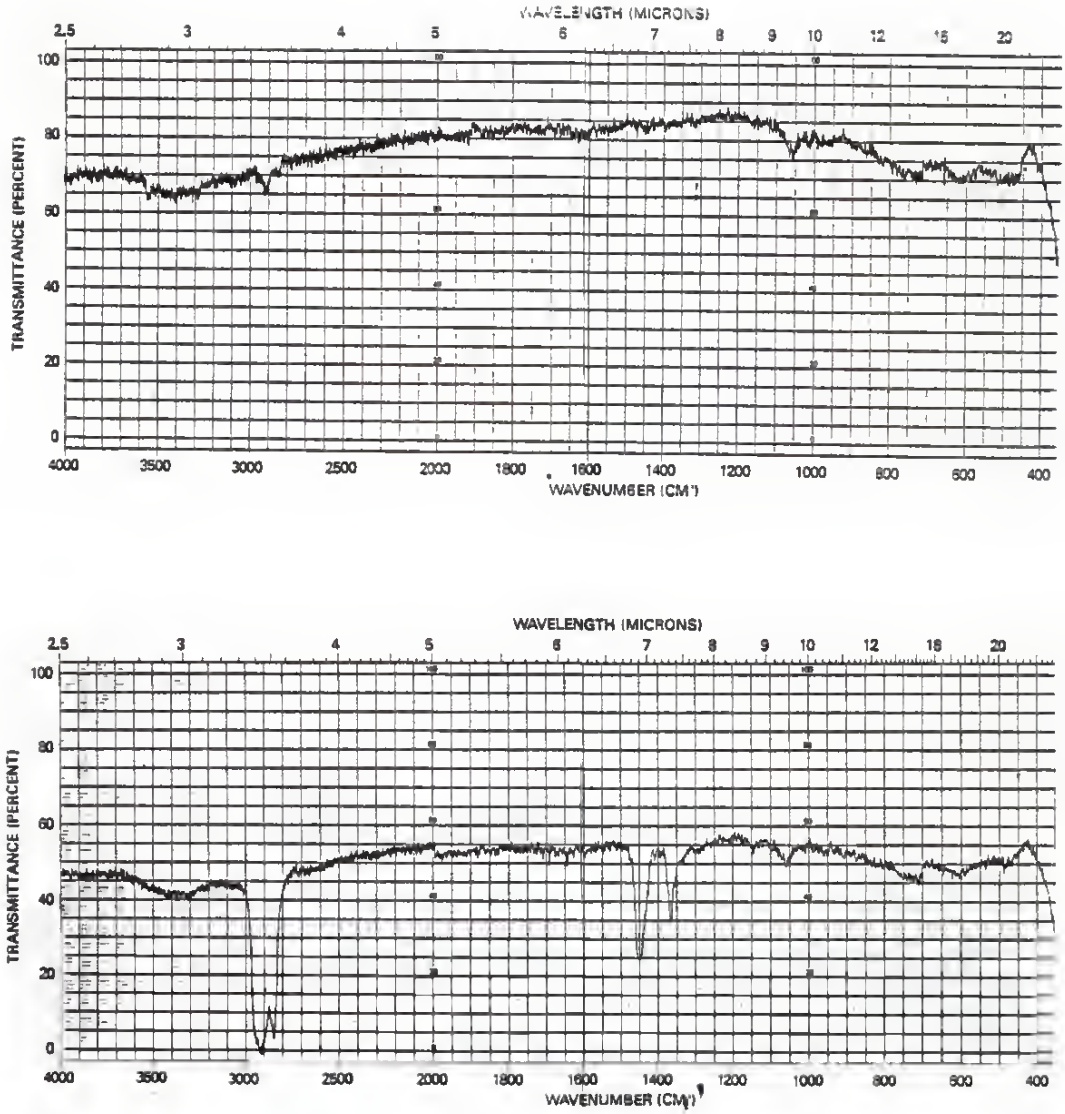

Figure 18. Mid-IR background spectra. Figure 18a is the spectrum of the blank KBr windows. Figure 18b is the spectrum of NUJOL between the KBr windows.

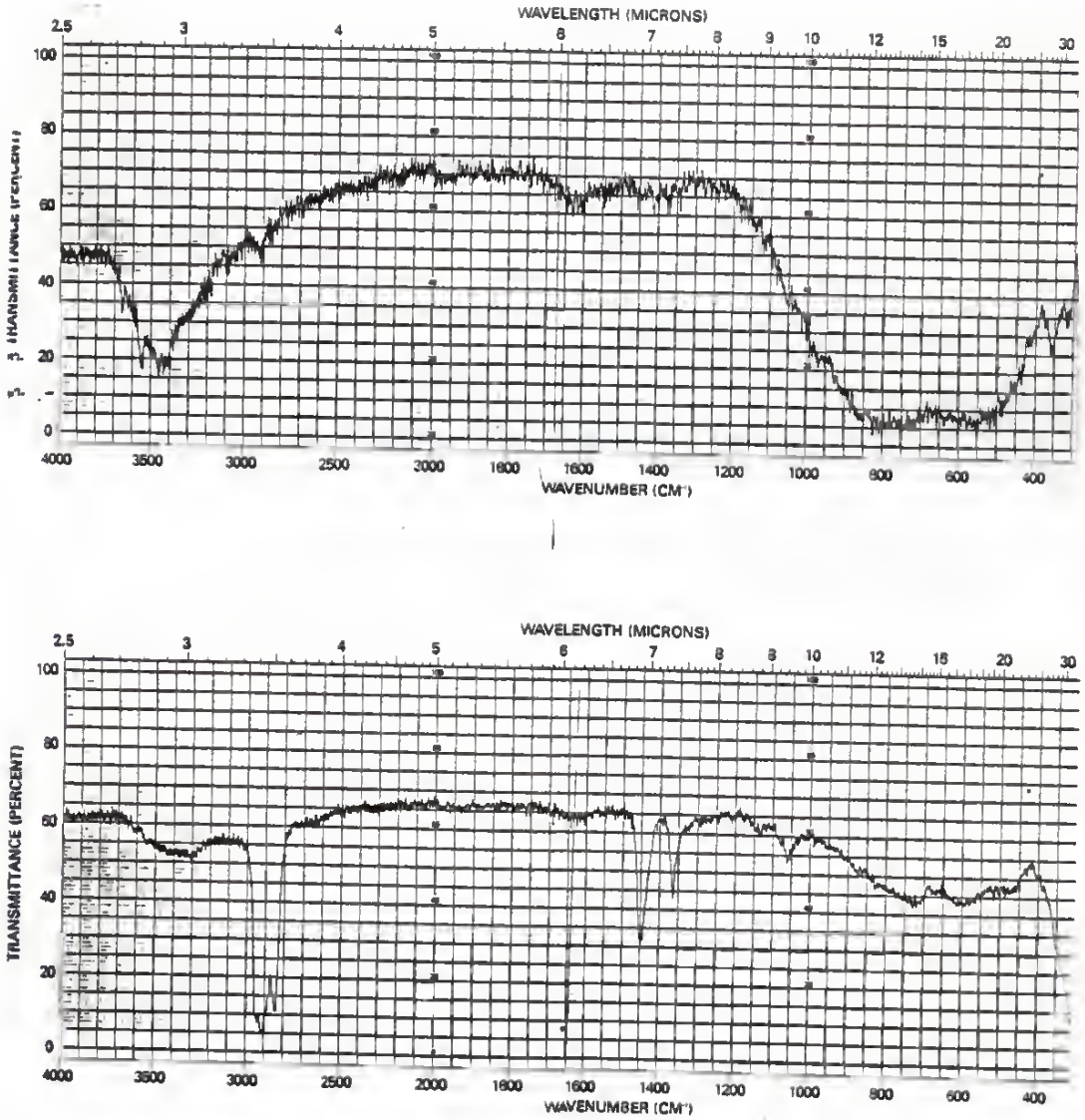

Figure 19. Bayerite mid-IR transmission spectra. 19a) is the spectrum of the sample prepared as a KBr wafer. 19b) is the spectrum of the sample prepared as a NUJOL mull.

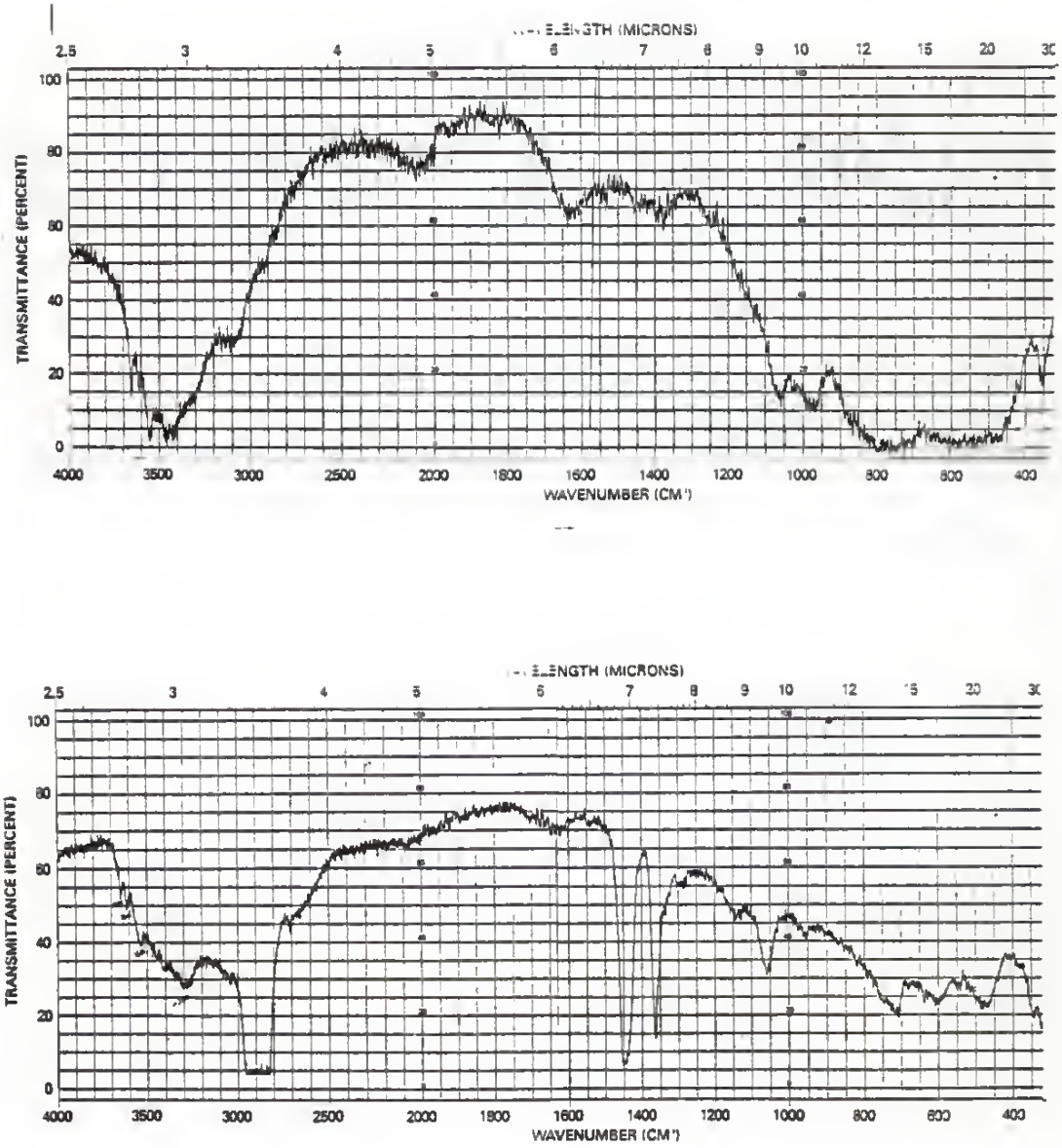

Figure 20. Boehmite mid-IR transmission spectra. 20a) is the spectrum of the sample prepared as a KBr wafer. 20b) is the spectrum of the sample prepared as a NUJOL mull.

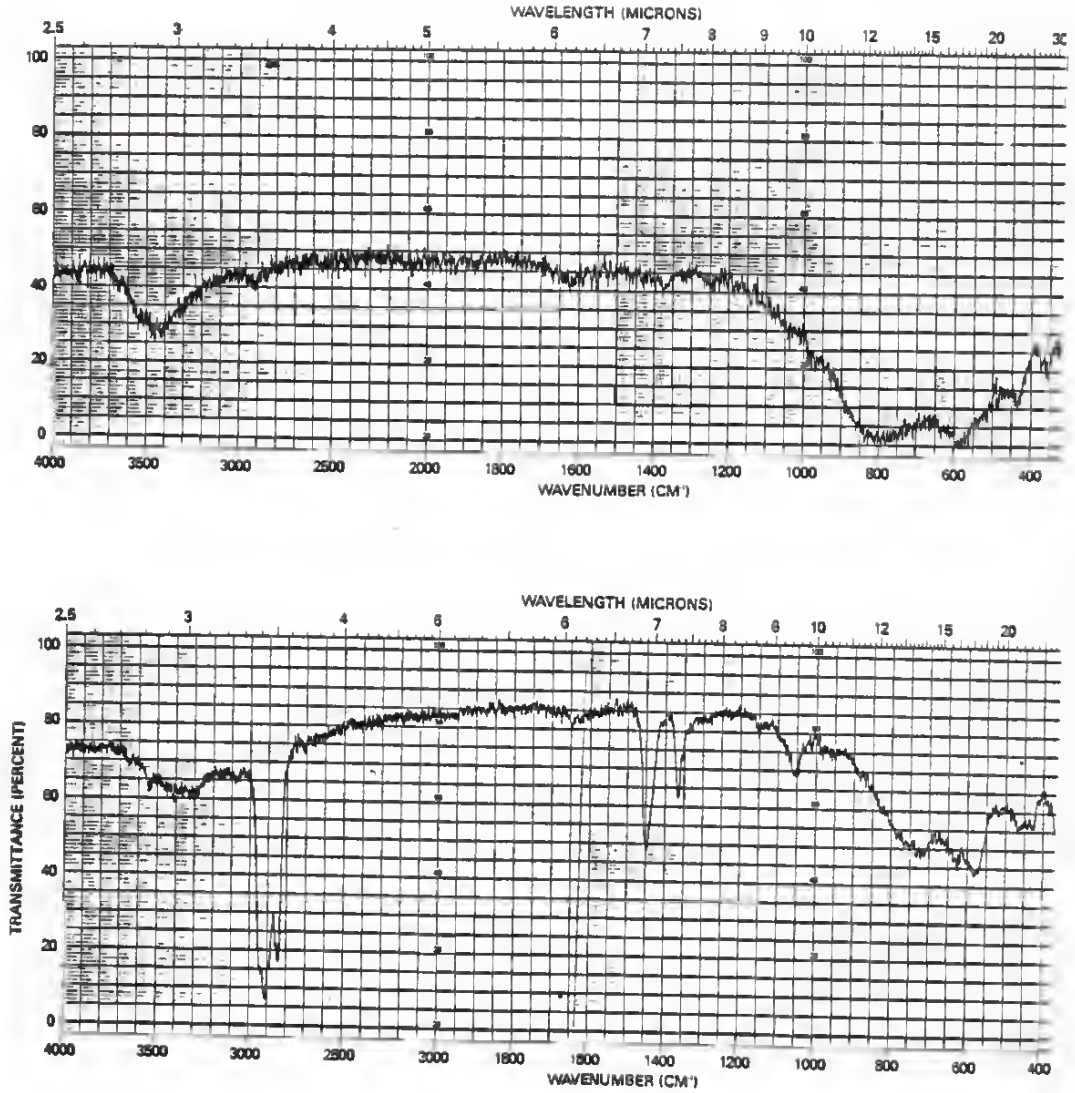

Figure 21. η-Alumina mid-IR transmission spectra. 21a) is the spectrum of the sample prepared as a KBr wafer. 21b) is the spectrum of the sample prepared as a NUJOL mull.

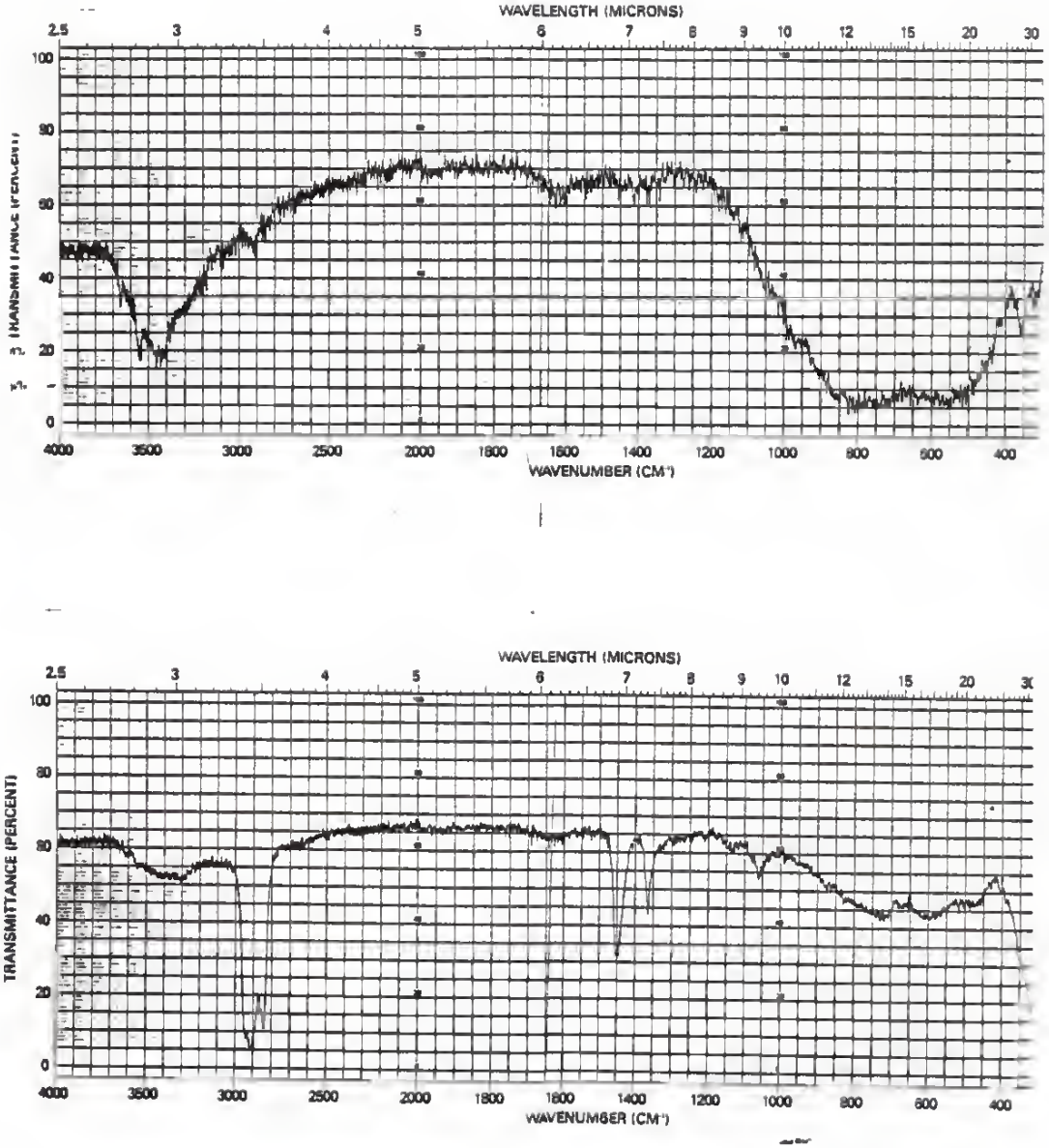

Figure 22. γ-Alumina mid-IR transmission spectra. 22a) is the spectrum of the sample prepared as a KBr wafer. 22b) is the spectrum of the sample prepared aa a NUJOL mull.

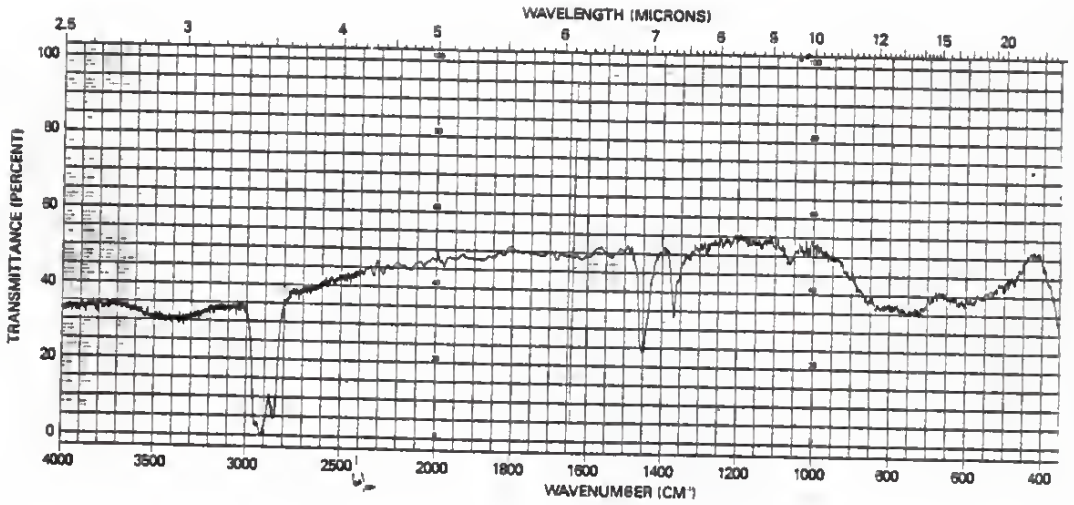

Figure 23. α-Alumina mid-IR transmission spectrum. The sample was prepared as a NUJOL mull.

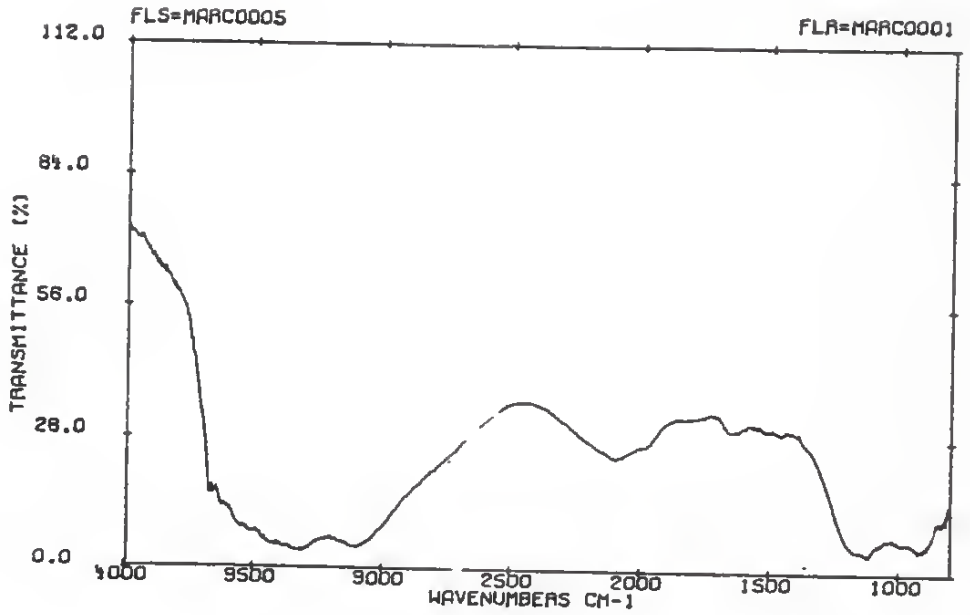

Figure 24. Boehmite (neat) mid-IR DRIFT spectrum.

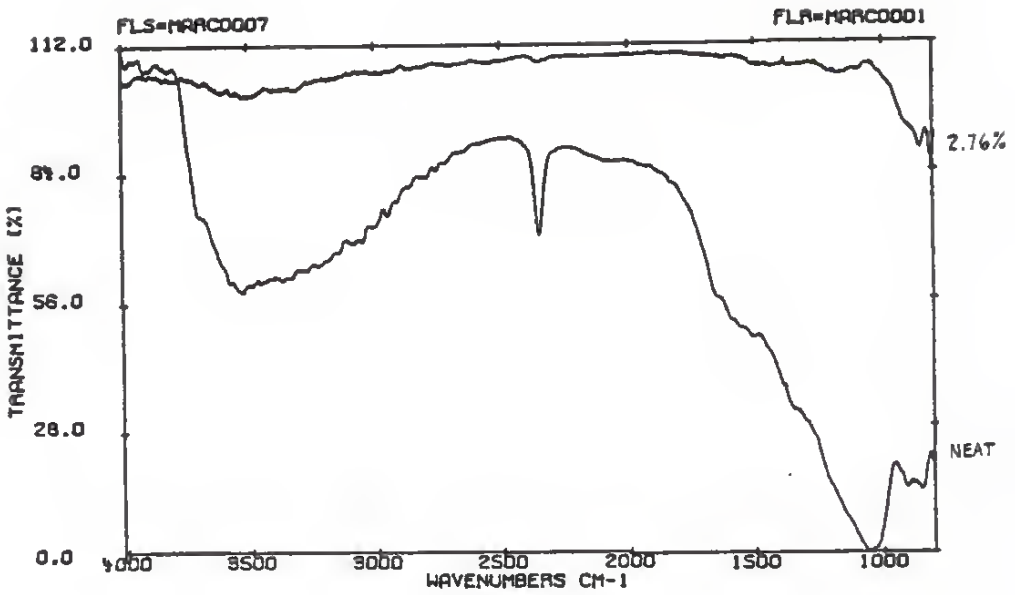

Figure 25. γ-Alumina (neat and 2.76% dilute alumina) mid-IR DRIFT spectra.

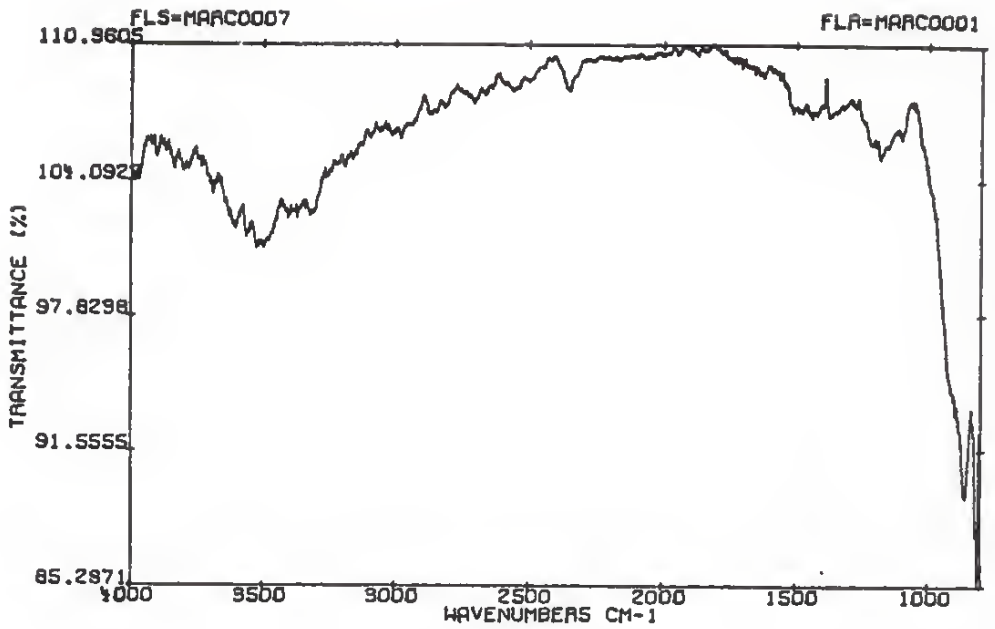

Figure 26. γ-Alumina (2.76% in KBr) mid-IR DRIFT spectrum.

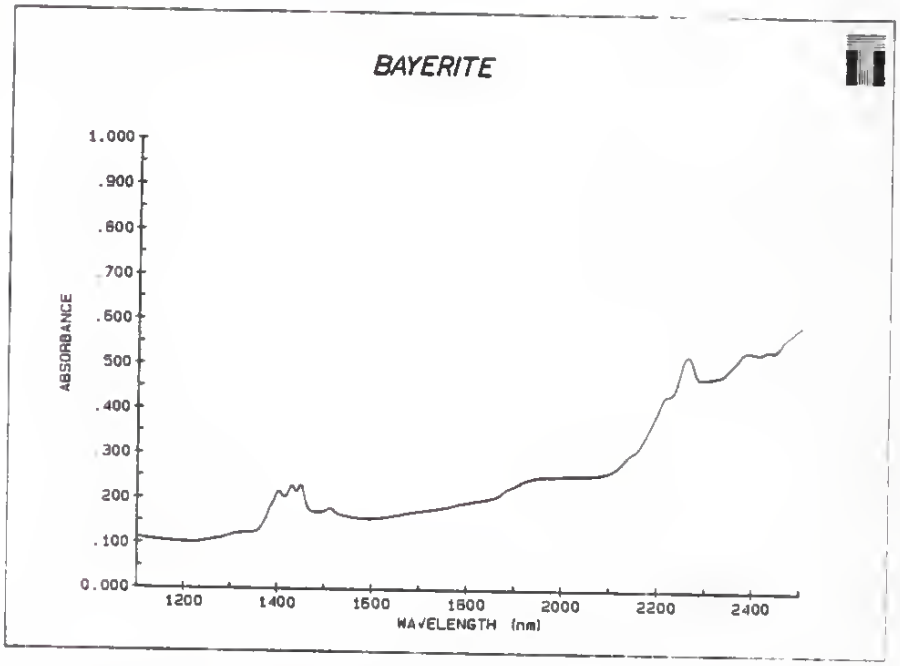

Figure 27. Bayerite (neat) near-IR DRIFT spectrum. A Technicon 500 spectrometer was used.

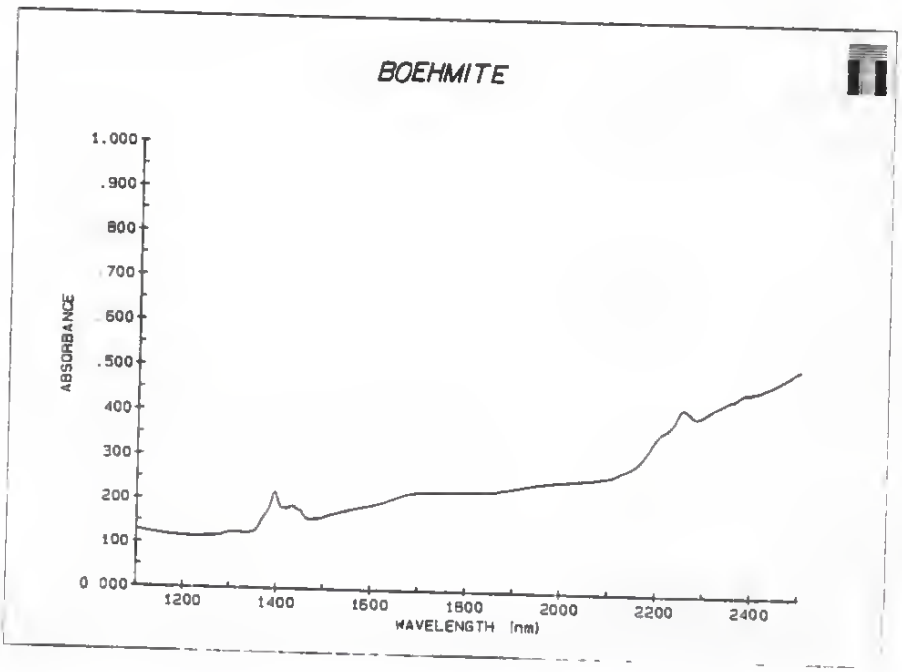

Figure 28. Boehmite (neat) near-IR DRIFT spectrum. A Technicon 500 spectrometer was used.

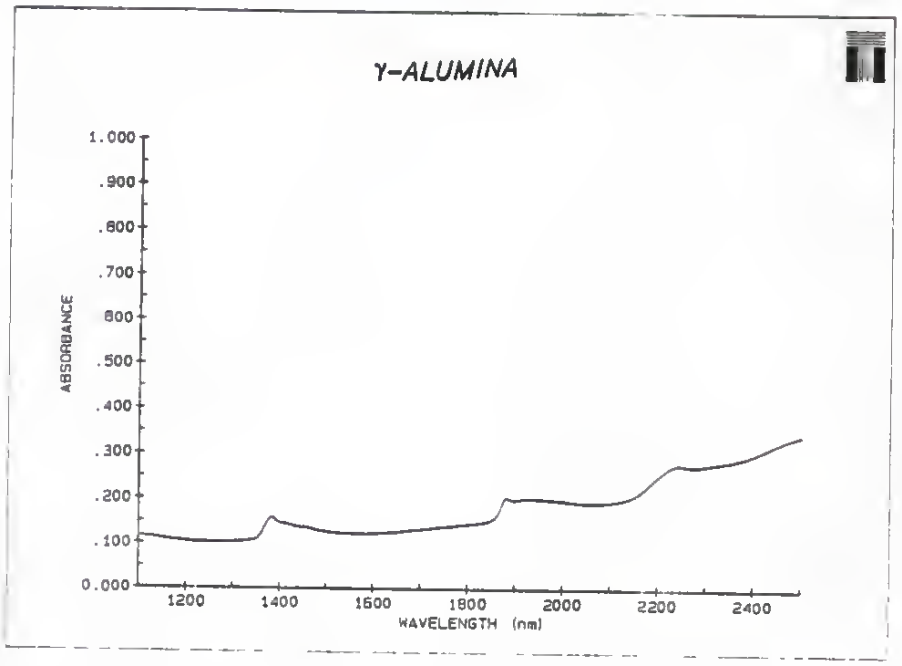

Figure 29 γ-Alumina (neat) near-IR DRIFT spectrum. A Technicon 500 spectrometer was used.

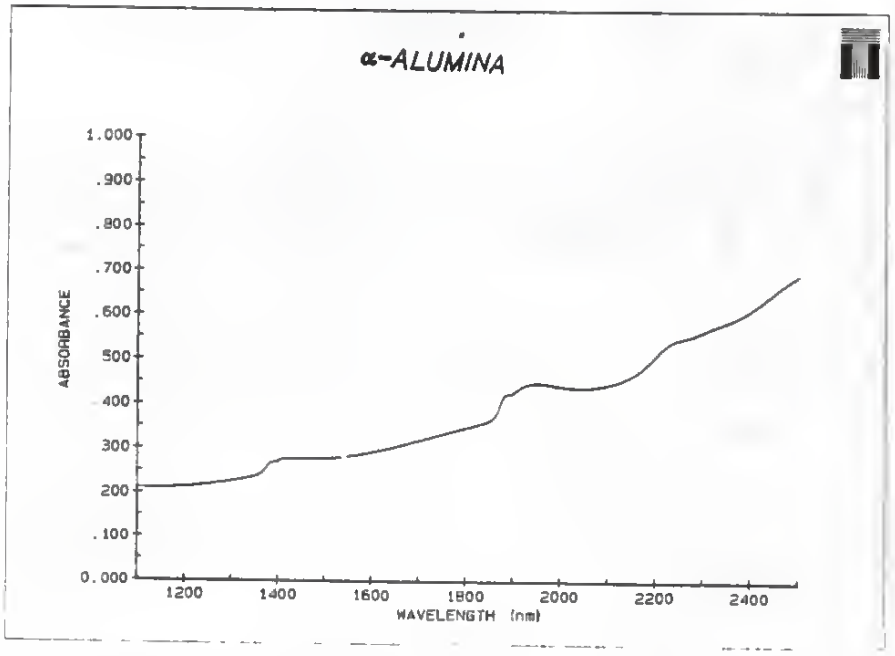

Figure 30 α-Alumina (neat) near-IR DRIFT spectrum. A Technicon 500 spectrometer was used.

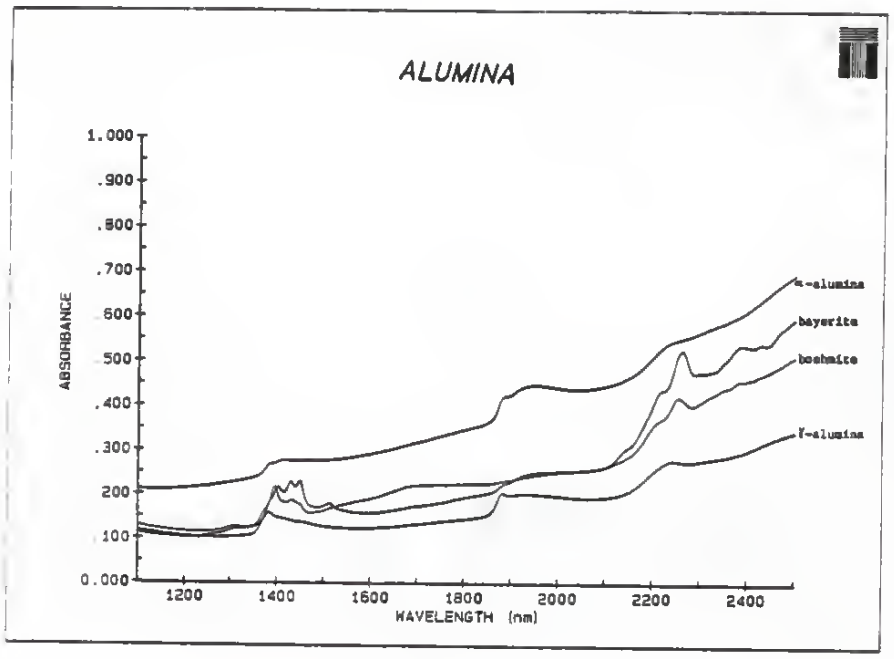

Figure 31 Consolidated plot of figures 26 to 30 illustrating the intensity of each of the spectrum relative to the others. The α-alumina particles are about one order of magnitude smaller in diameter than the other three samples.

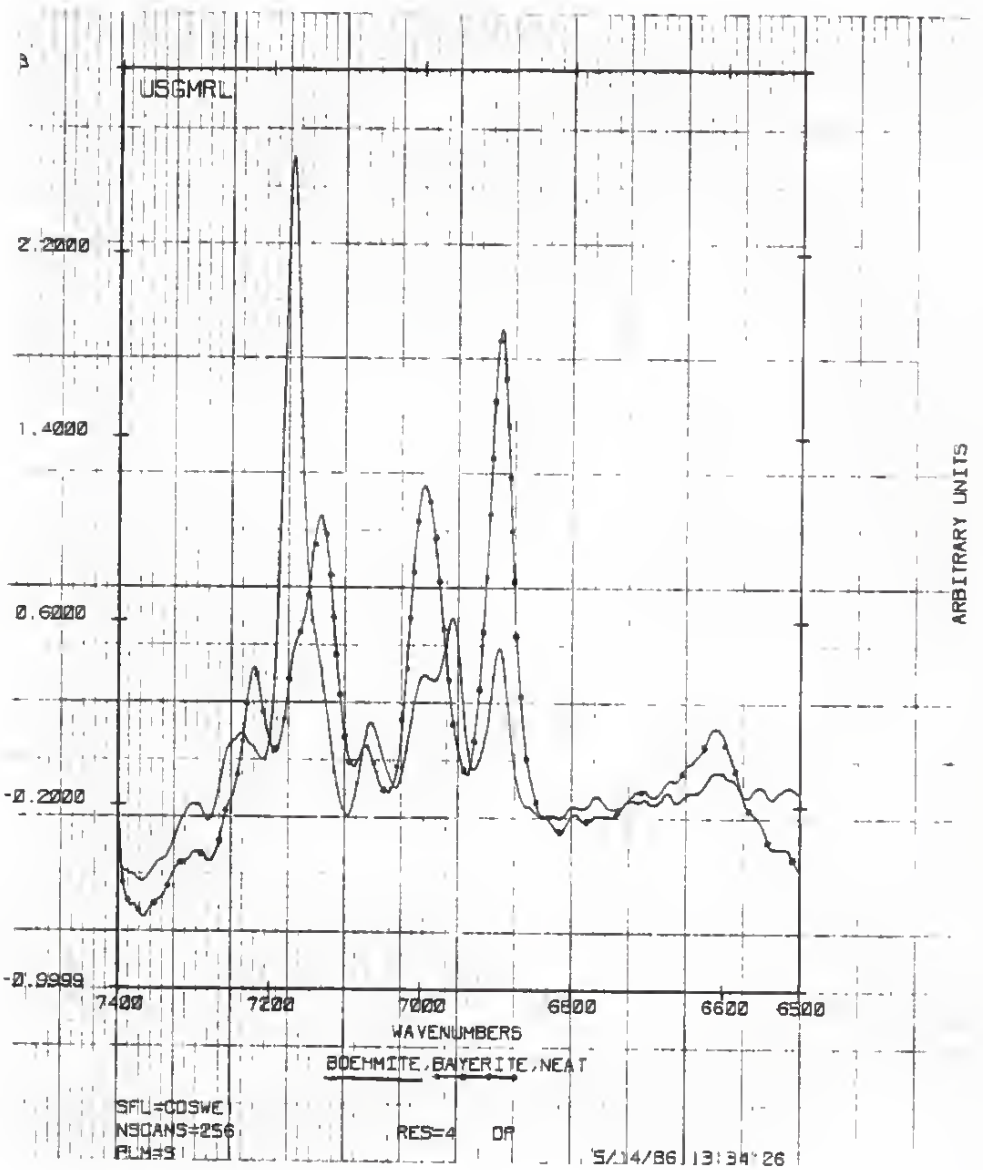

Figure 32 Bayerite and boehmite near-IR DRIFT spectra (DIGILAB 15S spectrometer).

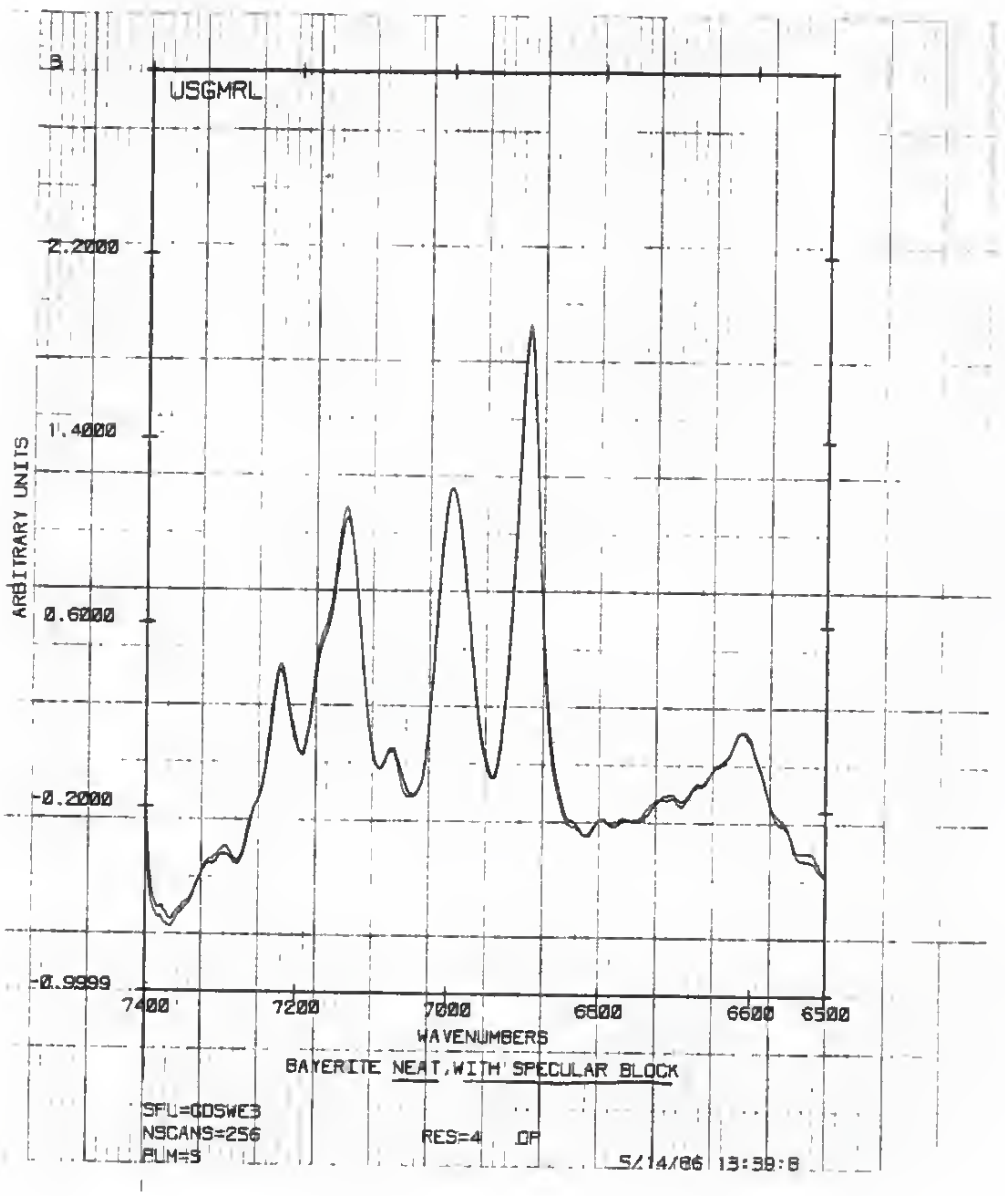

Figure 33 Bayerite near-IR DRIFT spectra (DIGILAB 15S spectrometer). The lower plot is the bayerite spectrum with the specular blocker in. The upper plot is the same sample with the blocker out. One third less counts were detected for the spectrum obtained with the specular blocker in place.

Chapter 7

Conclusions and Recommendations

7.1 Conclusions

DRIFT spectroscopy can be a valuable resource in the analysis of surfaces and inorganic catalysts. Coherent scattering from absorbing is present to some extent and must be handled. Coherent scattering will be minimized when fine particles are sufficiently seperated. The particle diameters must be less than or equal to the wavelength of the strong absortion band. An inert matrix is typically used to seperate the particles. Silicon is a better diluent for inorganics than KBr or KCl, since they are hygroscopic. When the coherent scattering is very low, the preponderence of the reflection will be diffuse. The only losses from the incident EM field are from absorption, giving a true absorption spectra.

Each of the formulas used in quantitative analysis are valid only for dilute sample concentrations. This reflects the severe coherent scattering effects that occur when coherent scattering becomes very significant. Multiple scattering from closely spaced particles which both absorb and scatter is well beyond current capabilities to model mathmatically.

The use of cross polarizers offers a possibility to extend the quantitative capabilities of DRIFT, if sufficient radiation can be provided in the infrared region of the spectrum. Both specular and diffuse Freshnel reflection are polarized and can therefore be eliminated by the second polarizer. A true absorption spectra can be

obtained be determining the amount of these two reflection components and eliminating them from the energy balance.

Current optical configurations which eliminate specular reflection cannot affect diffuse Freshnel reflection. Furthormore, the reflection is merely blocked, effectively adding this energy loss to the amount of energy that is absorbed. These spectra are often very similar to transmission spectra. Pressed wafers also exhibit specular reflection.

DRIFT spectroscopy can be performed on samples at higher concentrations for qualitative analysis. Difference spectra are an excellent way to analyze the molecular changes that occur as a result of a particular pertubation of the sample. Since the sample is not moved, the scattering properties remain the same throughout the experiment. The absorption bands which are unchanged by the pertubation will be eliminated by subtracting one spectra from the other.

The qualitative use of DRIFT can be broken into three areas. The first is the region far from the absorption band, where changes in the refractive index are not significant. This region should be acceptable for the qualitative analysis through the use of difference spectroscopy or time resolved spectroscopy. The second region is affected by the change of refractive index. It is essential to determine if the strong absorption from the lattice is reproduceable as the concentration of adsorbed surface species is altered. The region will provide useful information if the effects are reproduceable (difference spectroscopy techniques). The SNR will be relatively poor in this region, because much of the signal has been specularly reflected. The third region, which is distorted by the restrahlen band, is very difficult to analyze.

False peaks occur as a result of the inverted absorption peaks. Dilute spectra of the same sample may provide sufficient information to take advantage of this region. The mid-IR DRIFT of γ-alumina clearly demonstrated the usefulness of using a neat sample. The shoulder that was observed on the γ- alumina bydroxyl stretching band was not observed through any of the other techniques.

7.2 Recommendation for further research

The DRIFT in-situ chamber and the DRIFT accessory must be aligned. Once the interferomenter becomes operational, a small piece must be welded to the lower section of the cell to orient the chamber on the cradle precisely the same way each time. The piece will rest against one of the small brass rods of the cradle (chapter 4).

The cell design must be studied. The DRIFT in-situ chamber collects less radiation than a simple praying mantis accessory sample area, since the KBr exit window subtends less of the diffuse reflection area than the accessory collecting mirror. Samples should be analyzed using three different configurations of the in-situ chamber. First, the chamber should be used without the top section (no optical restriction of the radiation). Second, the top section should be placed on the chamber without the KBr windows. Finally, the complete chamber with windows should be used. At least two different samples should be irradiated, one possessing a very strong absorption band and the other a nonabsorber. Two key areas are involved. This experiment is designed

to determine if there is sufficient radiation throughput from the chamber to obtain a good SNR. This experiement is also designed to determine the change in the spectra that occurs by biocking specular reflection. The windows are positioned in different planes with the incident radiation, thereby eliminating any "mirror" refiection.

A major portion of the theory of this paper addressed coherent scattering. The sample concentration affects the particle separation and subsequentiy the coherent scattering. A series of spectra of the same sample shouid be taken at different concentration from about .1 to 100%. Both the quaiitative and quantitative nature of the spectra should be analyzed. Two questions shouid be answered. What is the concentration iimit for quantitative anaiysis by Kubeika-Munk or another equation? Is there a concentration iimitation to the qualititave use of the sampie? This second question deais with the distortion that takes place when the index of refraction increases and becomes complex. The γ-aiumina spectra mid-IR DRIFT spectra obtained in this research demonstrated some of the problems this causes in identifying the absorption peaks. These spectra aiso demonstrated that quite useful information is available for neat sampies.

The use of silicon as a diiuent shouid be studied. It would be best to take severai spectra at a series of concentrations. Both the quantitative and the qualitative capabilities shouid be assessed.

The dehydroxylation of bayerite to η-aiumina and boehmite to γ-alumina should be conducted and anaiyzed. The low temperature aluminas wouid be placed in the in-situ chamber sampie area. The post shouid then be stepwise elevated in temperature to 600°C. A vacuum shouid be

maintained in the chamber throughout the dehydroxylation. It is not known how much time is required for the transition to take place. Twenty-four hours in a muffle furnace is sufficient as evidenced by the samples prepared in this research. This experiment is designed to analyze the changes that occur in the hydroxyl groups during dehydroxylation. The purpose of the proposed research is to increase the understanding of the phase transition and subsequently the individual hydroxyl group sites. If silicon can be used as a diluent, the Al-O stretching mode absorptions could also be analyzed as a function of dehydroxylation.

Appendix 1

Fourier Transform Spectroscopy

Fourier transform spectroscopy:

Fourier transform spectroscopy differs significantly from the conventional dispersive spectroscopy. The entire spectral region of interest is detected continuously. The resulting interferogram does not resemble a conventional spectrum but it contains the same information. These are related mathematically through the Fourier integrals:

$$f(x) = \int_{-\infty}^{\infty} F(\nu) e^{2\pi i x \nu} \, d\nu \qquad (21)$$

and

$$F(\nu) = \int_{-\infty}^{\infty} F(\nu) e^{2\pi i x \nu} \, dx \qquad (22)$$

where f(x) is the interferogram or wave form and lies in the time or space domain. $F(\nu)$ is the spectra and lies in the frequency domain.

In practice, the limits of integration equation 22 are finite; ie., +s to -s. The truncation of the limits of integration results in a broadening of the peaks. A second result of truncation is the appearance of an extrema on each side of the primary feature. The interferogram can be multiplied by an appodization function to reduce these two effects.

Michaelson Interferometer:

An interferometer is used in Fourier transform spectrometers. In a Michaelson interferometer, the beam splitter divides split the incident beam and directs the beams toward two different mirrors (see figure 34). One beam travels to a fixed mirror, M_1, and is then reflected back to the beam splitter. The other travels to a moving mirror, M_2 and is reflected back. When the two beams recombine they constructively interfere forming an interferogram, S_1. The path length of the radiation which travels to the moving mirror is constantly varying linearly with time. The changing path length continuously alters the phase relationship between the two beams as they recombine. The fluctuating portion of the interferogram contains the spectral information and is the only portion of the interferogram which is Fourier transformed into the spectra.

An excellent book provides extensive information on the use of Fourier transform IR [30].

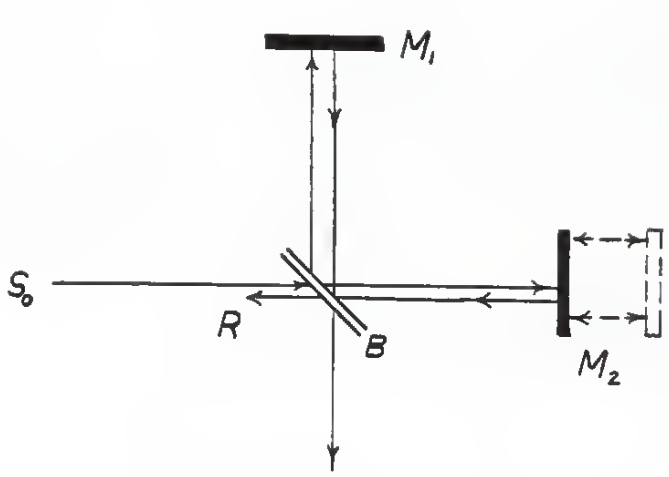

Figure 34. Schematic of a Michaelson interferometer. B is the beamsplitter. M_1 is the fixed mirror and M_2 is the moving mirror. S_0 is the incident beam and S_1 is the beam resulting from the recombination of the two reflected beams, the interferogram.

APPENDIX 2

Viewfactor of KBr Window

The author adapted a Monte Carlo statistical model to determine the viewfactor of the KBr "exit" window for radiation emmanated from the sample surface. A random point was chosen on the surface by selecting a random radius, r, and a random angle, Θ (0 to 2π). Two more random numbers were selected to identify the direction that a ray emmanated from that point would travel. The first , γ (0 to 2Π), is defined as the angle in the plane of the sample. The second , ϕ (0 to $\Pi/2$), is defined as the angle out of the plane. If the ray passed through the window, it was recorded as a hit. If not, it was recorded as a miss. This was repeated many times to establish a statistical base. The percentage of hits is, therefore, the probability that radiation from the surface will directly intercept the KBr window.

The following assumptions must be made. First, the radiation is diffusely emmanated from the sample surface. Second, there is equal probability that radiation will be emmanated from any point on the sample surface. This assumption is poor, but it should not affect the results significantly. A Gaussian distribution with respect to the center of the circle would be a better approximation.

The surface of the sample and the KBr windows were in two different planes, which intersected each other at 41°. No analytical solution was found for two disks in this orientation. Furthermore, this orientation leads to a complicated geometrical relationship between the two disks. One disk was therefore modeled as a sphere. A correction

factor was used to adjust the viewfactor for the extra hits recorded with the sphere. Since the sample area is smaller than the window in diameter and the viewfactors of two surfaces with respect to one another are related, the viewfactor of the sample area from the KBr window was calculated. The calculations were performed in the following order:

1) A random point was selected.

2) A random vector emmanating from this point was selected.

3) The distance from the random point to the center of the sphere was calculated.

4) A line segiment was constructed along the ray beginning at the random point.

5) The coordinates of the end point were calculated. These coordinates were then used to see if the point fell within the sphere. A hit was recorded if the criteria was met.

6) Steps one to five were repeated twenty thousand times for probability of .270 of directly intercepting the sample area.

Once the view factor of the sample area had been calculated, an appropriate correction factor was needed. The correction factor was needed, because the sphere has a larger projected area than a disk for some of the locations on the disk. The sphere and the disk were projected onto the plane which is perpendicular to the plane of the disk and which also passes through the center point of the sphere (see figure 35). Measurements were taken from this drawing (figure 35) to calculate the percentage of angles from each point that intercepted the sphere, but not the disk. These were misidentified as hits in the program. The percentages form each point were fit to a quadratic equation with the

dependent variable being the position on the line. The equation was then integrated over the entire length of the line to determine a correction function. 6.3% of the attempts were misidentified as hits. Therefore, the viewfactor of the sample area from the window equals .208.

Using the relationship:

$$A_1F_{12} = A_2F_{21} \tag{23}$$

where A_i is the area of "i" and F_{12} is fraction of diffuse radiation leaving A_1 that will be directly intercepted by A_2. F_{21} was calculated to be .318. Therefore, 31.8% of the diffuse radiation will contact the KBr window.

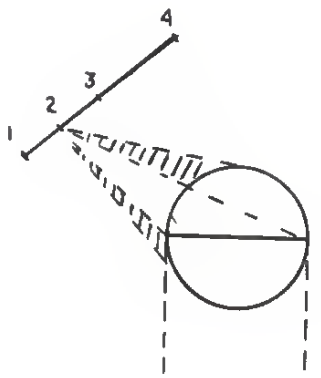

Figure 35. Viewfactor. This figure is a profile view of the sample cup and the KBr window of the in-situ DRIFT chamber. This projection was used to calculate a correction factor. Points 1 to 4 were selected on the projection of the window onto the plane. The percentage of radiation misidentified as hits was measured for each point.

Appendix 3

Thermocouple Calibration

The calibration tables in the CRC, Handbook of Chemistry and Physics [51], are designed for use with an appropriate correction factor. The correction factor, ΔE, is the difference between the observed and the standard. The E.M.F is not linear, therefore, the calibration is only valid when the cold junction is maintained at a temperature very close to the calibration temperature. The measurements are only valid when the DRIFT chamber is being cooled by tap water (19°C).

The micromelting point of crystalline materials was used to provide reference temperatures in calibrating the thermocouple (see Table 8).

Table B.

Calibration Table

Material	Melting point	Measured E.M.F.	Standard E.M.F.	ΔE
9,10 Dihydroanthraene	104°-107°C	3.43	5.56	2.13
Benzoic acid	122.13°C	4.25	6.47	2.445
Benzamide	132°-133°C	4.29	7.04	2.75
Sucrose	185°C-186°C	7.38	9.97	2.59
Potassium Dichromate	398°C	17.4	21.74	4.34

The correction factor ΔE is plotted versus temperature. Thc data fits the following curve:

$$\Delta E = 1.54 + .00695 \cdot T \quad (mv) \qquad (24)$$

with a correlation of .972. The standard curve (cold junction at 0°C) and the measured curve are plotted (see figure 36).

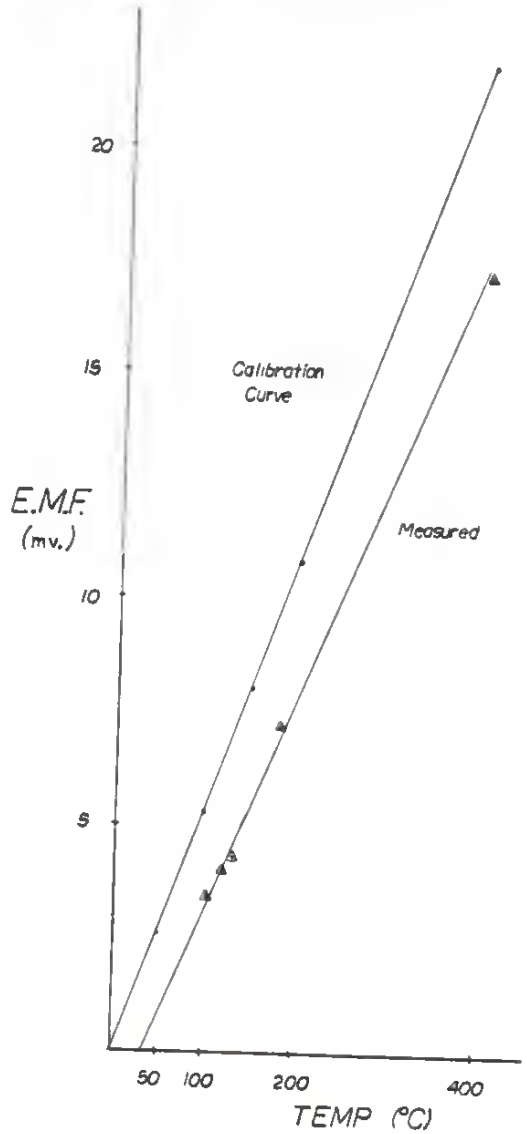

Figure 36. Calibration chart for the thermocouple. The lower curve is for the measured values. The upper curve is for the standard calibration. The difference, ΔE is the correction factor.

References

1. R. P. Elchens, W. A., Pliskin, Adv. Catal. 10, 1 (1958).

2. Alexis T. Bell, In Vibrational Spectroscopy for Adsorbed Species, Alexis T. Bell and Michael L. Hair, Eds., American Chemical Society, Washington D.C, 1980, Chap.2.

3. Gary T. Haller, Catal. Rev. - Sci. Eng. 23(4), 477 (1981).

4. J. B. Peri, J. Phys. Chem., 69, 231 (1965).

5. Kenzi Tamaru and Takaharu Onishi, Appl. Spec. Rev. 9(1), 233, (1975).

6. Peter R. Griffiths Howard J. Sloane and Robert W. Hannah, Appl. Spec. 31, 485 (1977).

7. R. R. Willey, Appl. Spec., 30, 593 (1976).

8. Michael P. Fuller and Peter R. Griffiths, Am. Lab., 10(10),69 (1978).

9. D. Kuehl and P. R. Griffiths, Anal. Chem. 52, 1354 (1980).

10. S. Agyare Yeboah, Shih-Hsien Wang and Peter R. Griffiths, Appl. Spec. 38, 259 (1984).

11. M. Nanzyo, J. Soil Sci. 35, 63 (1984).

12. Isaam M. Hamadeh, Ph. D. Dissertation, Ohio University, Athens Ohio (1982).

13. Paul J. Brimmer, Peter R. Griffiths and N. J. Harrick, Appl. Spec. 40, 258 (1986).

14. Francis A. Jenkins, and Harvey E. White, Fundamentals of Optics, McGraw Hill, New York, 1976.

15. Arthur W. Adamson. A Textbook of Physical Chemistry,Academic Press, New York, 1973.

16. Al Compaan, personal communication with, Kansas State University, Manhattan Kansas, 1985.

17. Robert Hamacker, personal communication with, Kansas State University, Manhattan Kansas, 1985.

18. Gustav Kortüm, Reflectance Spectroscopy, Springer-Verlag, New York, 1969.

19. James Macomber, The Dynamics of Spectroscopic Transitions, Wiley, New York, 1976.

20. Jeanette G. Grasselli, Marcia K. Snavely and Bernard Bulkin, Chemical Applications of Spectroscopy, Wiley New York, 1981.

21. Richard P. Feynman, Robert P. Leighton and Matthew Sands, Feynman Lectures on Physics, Addison-Wesley, Reading, Mass., 1963.

22. Teiki Iwaoka, Shih-Hsien Wang and Peter R. Griffiths, Spectro. Acta, 41A, 37 (1985).

23. Peri, J. B., in Catalysis, John R. Anderson and Michel Boudart, Eds., Springer-Verlag, Berlin, 1984, Chap 3.

24 A. Ahmed and E. Gallei, Appl. Spec., 28,430 (1974).

25. G. Laufer, J. T. Huncke, B. S. H. Royce and Y. C. Teng, Appl. Phys. Letters 37, 517 (1980).

26. J. B. Peri, J. Phys. Chem., 69, 211 (1965).

27. J. B. Peri and R. B. Hannan, Spect Acta 16, 237 (1960).

28. R. Byron Bird, Warren E. Stewart and Edwin N. Lightfoot, Transport Phenomena, Wiley, New York, 1960.

29. Michael P. Fuller and Peter R. Griffiths, Anal Chem. 50, 1906 (1978).

30. Peter R. Griffiths and James D. Haseth, Fourier Transform Infrared Spectrometry, Wiley, New York, 1986.

31. Issam M. Hamadeh, Dewey King and Peter R. Griffiths, J. Catal. 88, 264 (1984).

32. Robert G. Messerschmidt, Scan Time, 7, 1, (1985).

33. Harry G. Hecht, Appl. Spec. 30, 610, (1976).

34. A. Schuster, Astrophys. J., 21, 1, (1905).

35. S. Chandrasekhar, Radiative Transfer, Clarendon Press, Oxford, 1950.

36. Harry G. Hecht, Appl Spec. 37, 348 (1983).

37. Grovanelli, R. G., Opt. Acta 2, 4 (1955).

38. E. Pitts, Phys. Soc. of London Proc. 67, 105 (1954).

39. Paul Kubelka, J. Opt. Soc. Am., 38, 448 (1984).

40. P. Kubelka, and F. Munk, Zeits f. tech Physik, 12, 593 (1931).

41. Harry G. Hecht, Appl. Spec., 34, 161, (1980).

42. Hecht and Zajack

43. Charles Kittel, Introduction to Solid State Physics, Wiley, New York, 1966.

44. R. P. Eichens, W. A. Pliskin and S. A. Francis, J. Phys. Chem., 22, 1786, (1954).

45. L. H. Little, Infrared Spectra of Adsorbed Species, Academic Press, New York, 1966.

46. M. L. Hair, Infrared Spectroscopy in Surface Chemistry, Dekkar, New York, 1967.

47. R. F. Hicks, C. S. Kellner, B. J. Savatsky, W. C. Hecker and A. T. Bell, J. Catal. 71, 216, (1981).

48. M. Niwa, T. Hattori, M. Takahashi, K. Shirai, M. Watanabe and Y. Murakami, Anal. Chem., 51, 46 (1979).

49. Harrick Scientific Corp., fact sheet that accompanies the HVC-DRP in-situ DRIFT chamber, P.O. Box 867, Ossining New York,

50. William R. Moser, Chen-Choo Chiang and Robert Messerschmidt, Scan Time, 7, 1, (1985).

51. Robert C. Weast, Handbook of Chemistry and Physics, 55th edition, CRC Press, 1974.

52. Lawrence Sampson, M. S. Thesis, Kansas State University, Manhattan Kansas, (1985).

53. Bruce C. Gates, James R. Katzer and G. C. A. Schuit, Chemistry of Catalytic Processes, McGraw Hill, New York, 1969.

54. Karl Wefer and Gordon M. Bell, Oxides and Hydroxides Technical Paper No. 19, ALCOA Research Laboratories, 1972.

55. W. D. Kingery, H. K. Bowen and D. R. Uhlmann, Introduction to Ceramics, Wiley, New York.

56. Leo D. Frederickson, Jr. Anal. Chem. 26, 1883 (1954).

57. J. L. Carter, P. J. Luchesi, P. Corneil, D. J. C. Yates and J. H. Sinfelt, J. Phys. Chem. 69, 3070 (1965).

58. Sadtler Research Lab.

59. V. A. Kolesova, Opt. Spektrosk, 6, 20, (1959).

60. Robert M. Silverstein Robert M, Clayton G. 8assler and Terence C. Morrill, Spectrometric Identification of Organic Compounds. Wiley: New York, 1981.

61. J. 8. Peri, J. Phys. Chem., 69, 220 (1965).

62. 8. C. Lippens and J. J. Steggerda, in Physical and Chemical Aspects of Adsorbents and Catalysts (B. G. Linsen, ed.), Academic, 1970, p. 171.

63. Helmüt Knozinger, Advances in Catalysis, 25, 184 (1976).

64. M. Nanzyo, J. Soil Sci. 35, 63 (1984).

65. J. 8. Peri, J. Phys. Chem., 70, 3188 (1966).

66. W. M. Grim, III, J. A. Graham and W. G. Fately, Transform Times 1, 1 (November, 1983).

67. I. 8en-Gera and K. H. Norris J. Food Sci., 33 64 (1968).

68. K. H. Morris, R. F. 8arnes, J. E. Moore and J. S. Shenk, J. Anim. Sci. 43 ,889 (1978).

69. K. Klier, in Vibrational Spectroscopies for Adsorbed Species (Alexis T. 8ell and Michael L. Hair, ed)., American Chemical Society, New York 1980.

70. Daniel J. Pasto and Carl R. Johnson, Organic Structure Determination Prentice Hall, Englewood Cliffs, NJ., 1969.

71. Paul R. Matthewson, Ph. D. Dissertation, Kansas State University, Manhattan Kansas (1985).

72. Aaron Barkatt and Catherine J. Simmons, J. Phys. Chem., 85, 1824, (1981).

73. D. H. Strome and K. Klier, in Adsorption and Ion Exchange with Synthetic Zeolites, William H. Flan, Ed., American Chemical Society, Washington, D.C. 1980, Chap. 8.

74. A. Lee Smith, Applied Infrared Spectroscopy, Wiley, New York, 1979.

75. Larry Glasgow, course on Transport Phenomena, Kansas State University, Manhattan Kansas, 1986.

76. H. Knözinger and P. Ratnasamy, Catal. Rev.- Sci. Eng. 17(1), 31 (1978).

THE USE OF DIFFUSE REFLECTANCE INFRARED SPECTROSCOPY IN THE STUDY OF ALUMINA

by

MARC KEVIN COLLINS

B. S., United States Military Academy, 1977

AN ABSTRACT OF A MASTER'S THESIS

submitted in partial fulfillment of the

requirements for the degree

MASTER OF SCIENCE

Department of Chemical Engineering

KANSAS STATE UNIVERSITY
Manhattan, Kansas

1986

ABSTRACT

The purpose of this research was to determine the theoretical limitations which exist for the use of in-situ diffuse reflectance Fourier transform (DRIFT) spectroscopy to study alumina. Clear definitions were sought for the terminology used to explain reflectance, scattering and absorption.

The IBM FT-IR spectrometer and the IBM praying mantis DRIFT accessory have been modified to accept a Harrick in-situ DRIFT chamber. This chamber has been designed by Harrick for use at elevated temperatures with a controlled atmosphere.

Diffuse reflectance spectroscopy is limited by coherent scattering. Quantitative analysis with DRIFT is limited to dilute sample concentrations, in order to separate the particles adequately to avoid coherent scattering. The particle diameter should be less than or equal to the wavelength of the highest energy lattice stretching mode. Since alkyl halides are hygroscopic, silicon is a better diluent for DRIFT spectroscopy of oxides.

Neat alumina samples can be qualitatively used for DRIFT spectroscopy. Difference spectroscopy should provide useful information throughout most of the mid-IR region. When the wavelength is greater than about 8μm, the spectra is distorted by the restrahlen band. More research is required to determine if valid qualitative information can be extracted from spectra obtained with neat samples in this region.